UNIVERSITÉ DE MONTRÉAL

QUANTIFYING RARE EARTH ELEMENT CONTENT IN HIGH CONCENTRATED SAMPLES BY k_0-NAA

MARYAM ABDOLLAHI NEISIANI

DÉPARTEMENT DE GÉNIE CHIMIQUE

ÉCOLE POLYTECHNIQUE DE MONTRÉAL

MÉMOIRE PRÉSENTÉ EN VUE DE L'OBTENTION

DU DIPLÔME DE MAÎTRISE ÈS SCIENCES APPLIQUÉES

(GÉNIE CHIMIQUE)

AOÛT 2017

© Maryam Abdollahi Neisiani, 2017.

UNIVERSITÉ DE MONTRÉAL

ÉCOLE POLYTECHNIQUE DE MONTRÉAL

Ce mémoire intitulé:

QUANTIFYING RARE EARTH ELEMENT CONTENT IN HIGH CONCENTRATED SAMPLES BY k_0-NAA

présenté par : ABDOLLAHI NEISIANI Maryam

en vue de l'obtention du diplôme de : Maîtrise ès sciences appliquées

a été dûment accepté par le jury d'examen constitué de :

M. PATIENCE Gregory S., Ph. D., président

Mme CHILIAN Cornelia, Ph. D., membre et directrice de recherche

M. CHAOUKI Jamal, Ph. D., membre et codirecteur de recherche

M. SAMULEEV Pavel, Ph. D., membre

DEDICATION

To my loving family

ACKNOWLEDGEMENTS

I would like to extend my sincerest thanks and appreciation to those who helped me accomplish this study.

Undoubtedly, my supervisors Dr. Cornelia Chilian and Dr. Jamal Chaouki deserve to be at the top of the list. I would like to recognize Dr. Jamal Chaouki for giving me the opportunity to join his research team, for his support and encouragements. I would like to extend my gratitude to Dr. Cornelia Chilian, for her kind guidance, helpful suggestions, for her positive attitude and her patience. These past few years have been helpful in my academic progress.

I would like to express my deep sense of gratitude to all my committee members for accepting to be a member of my jury, namely, Dr. Pavel Samuleev and Dr. Gregory Patience.

I would like to acknowledge Natural Sciences and Engineering Research Council of Canada (NSERC) and Niobec, a Magris Resources Company, for funding this research. Special thanks to Dominic Downey from management team in Niobec for their guidance and support.

I would like to thank Cristina Cimpan for helping me to fulfill the experimental work during my first year in the laboratory.

I would like to extend my thanks to my colleagues and friends for sharing their friendship and knowledge with me. In addition, the members of the REE project group and especially to the project manager of the group Dr. Mohammad Latifi, the members of PEARL group, and everyone at SLOWPOKE.

Special thanks go to the secretaries and entire technical staff of the chemical engineering department and nuclear engineering department.

Finally, special recognition goes out to my family, for their support, encouragement and patience. To my incredible sister, Mania for encouraging me to reach the end of my potential and for believing in me. Your perseverance and hard work, your wisdom, your sense of discipline and above all, your love and patience, make you a real source of inspiration. To Rouzbeh, my brother in law who provided encouragement and support during the entire process as well as

continuously proofing my documents. To my sister Mitra, who always got my back during hard times with her support and love even though we were far apart.

I dedicate this thesis to my family and sincerely seek their blessing for the path ahead.

- به کجا چنین شتابان؟

- به هر آن کجا که باشد به جز این سرا، سرایم

Maryam Abdollahi Neisiani
August 2017
École Polytechnique de Montréal

RÉSUMÉ

Les terres rares (REEs) sont représentés par les éléments de la série des lanthanides incluant le scandium et yttrium. Actuellement, une grande attention est donnée aux REEs à cause de leur application dans plusieurs domaines de pointe. Dans ce contexte il y a un besoin accru pour des techniques analytiques capables de caractériser une gamme large de concentrations, en commençant avec les minéraux de faible concentration, jusqu'à leur raffinage; donc ayant des hautes concentrations en REEs. Cet étude se propose d'évaluer la performance de la méthode d'analyse par activation neutronique k_0 (k_0-NAA) appliquée dans le Laboratoire d'analyse par activation neutronique de Polytechnique Montréal pour la détermination avec précision des REE dans des matrices minérales de haute concentration. Les principaux facteurs qui influencent la méthode ont été investigués, en incluant les données nucléaires, la température dans les sites d'irradiation, les interférences nucléaires et spectrales, l'atténuation mutuelle des rayons gamma ainsi que l'autoprotection contre les neutrons. Afin de réaliser cet objectif, des échantillons mono-élément préparé avec des solutions standard certifiées et des oxydes standard certifiés ont été irradiés, comptés et analysés. Finalement, les protocoles d'analyse ont été optimisés en termes d'irradiation, décroissance et comptage afin de réduire le temps total d'analyse. Les incertitudes introduites par les facteurs mentionnés plus haut ont été évaluées. La capacité globale de la méthode améliorée k_0-NAA pour les REEs a été mise en œuvre avec un matériel standard certifié du Projet canadien pour la certification des matériaux de référence (REE-2) avec des concentrations de 7.2 mg kg^{-1} pour Yb jusqu'à 9610 mg kg^{-1} pour Ce. Les concentrations des REEs ont été mesurées avec des incertitudes plus faibles que 7% (à 95% intervalle de confiance) et ont été consistantes avec les concentrations spécifiées dans la certification du REE-2.

ABSTRACT

The rare earth elements (REE) are comprised of lanthanide series, from lanthanum to lutetium plus scandium and yttrium. Due to the rising applications of REEs in different fields of technology a lot of attention has been drawn to the extraction of these elements. Therefore, a reliable and accurate characterization technique is required to determine variable levels of REEs starting from mineral matrices all the way to processed samples. The aim of this work is to evaluate the capability of k_0-neutron activation analysis (k_0-NAA) implemented at Polytechnique Montreal for accurate determination of rare earth elements in high concentrated mineral matrices. Individual factors affecting the measurements including nuclear data used for the calculations, neutron temperature effects, nuclear interferences, spectral interferences, gamma-ray self-attenuation and neutron self-shielding were investigated. Mono rare earth element standard solutions and rare earth oxides were used to investigate these phenomena separately. Several improvements were applied to the current method. Analysis protocols were optimized in terms of irradiation, decay and counting times to obtain accurate results in shorter turnaround times, and uncertainty contributions from aforementioned factors were evaluated. To validate the overall capability of the improved k_0-NAA method for REE, a certified reference material (CRM) from Canadian Certified Reference Materials Project (REE-2) with REE content ranging from 7.2 mg kg^{-1} for Yb to 9610 mg kg^{-1} for Ce was used. The REE concentration was determined with uncertainty below 7% (at 95% confidence level) and proved to be consistent with the CRM certified concentrations.

TABLE OF CONTENTS

DEDICATION III

ACKNOWLEDGEMENTS IV

RÉSUMÉ VI

ABSTRACT VII

LIST OF TABLES XI

LIST OF FIGURES XIII

LIST OF SYMBOLS AND ABBREVIATIONS XIV

CHAPTER 1 INTRODUCTION 1

1.1 Context 1

1.1.1 Rare earth elements 1

1.1.2 Analytical techniques 4

1.2 Objective 6

1.3 Plan of the dissertation 6

CHAPTER 2 LITERATURE REVIEW AND THEORETICAL ASPECTS OF NEUTRON ACTIVATION ANALYSIS 7

2.1 Introduction 7

2.1.1 Advantages of neutron activation analysis 7

2.1.2 Drawbacks of neutron activation analysis 7

2.1.3 Principles of neutron activation analysis 8

2.2 Methods of standardization 18

2.2.1 Absolute standardization 18

2.2.2 Relative method of standardization 19

2.2.3 Comparator method of standardization 20

2.2.4 k_0-method of standardization 21

2.3 Equipment 22

2.3.1 Nuclear reactors 22

2.3.2 The counting system 25

2.3.3 Detectors 25

CHAPTER 3 SPECIFIC OBJECTIVES AND METHODOLOGICAL ASPECTS 28

3.1 Sources of error 28

3.1.1 Nuclear data, detection efficiency 29

3.1.2 Interferences 30

CHAPTER 4 EXPERIMENTAL METHODOLODY 38

4.1 Experimental procedures 38

4.2 Spectra analysis 39

4.2.1 EPAA 39

4.2.2 Iterative gamma-ray self-attenuation correction 39

4.2.3 Iterative neutron self-shielding correction 40

4.3 SLOWPOKE reactor 40

CHAPTER 5 ARTICLE 1: QUANTIFYING REE CONTENT IN HIGH CONCENTRATED SAMPLES BY K_0-NAA 42

5.1 Introduction 42

5.2 Experimental 46

5.3 Results and discussion 48

5.3.1 Sensitivity factors and EPAA libraries 48

5.3.2 Gamma-ray self-attenuation and Neutron self-shielding 58

5.3.3 Validation of k_0-NAA for REEs 60

5.4 Conclusions 63

5.5 Acknowledgements 63

5.6 References 63

CHAPTER 6 GENERAL DISCUSSION AND COMPLEMENTARY NAA RESULTS 65

6.1 Fresh ore and concentrated ore 66

6.2 Beneficiation of fresh ore: Froth flotation 68

CHAPTER 7 CONCLUSION AND RECOMMENDATIONS 71

BIBLIOGRAPHY 72

LIST OF TABLES

Table 1-1 Selected end-uses of rare earth elements 3

Table 4-1 SLOWPOKE design specifications 41

Table 5-1 Nuclear properties of REE radio isotopes used in this work: gamma energies (γ), k_0 and Q_0 values for target (TI) and formed isotopes (FI).....49

Table 5-2 Concentrations for the REE solutions on filter paper (X_p), normalized with respect to the standard certified values (X_{cert}) and corresponding coincidence summing correction factors (COI) for three different counting positions P1, P2 and P3 51

Table 5-3 Spectral Interference Correction Factors for three different counting positions, (P1, P2, P3) 56

Table 5-4 Uranium Fission Interference Correction Factors for REEs.....57

Table 5-5 Comparison of REE concentrations in oxides measured at different steps of k_0-NAA with respect to the certified values (X_{cert}): concentration obtained from EPAA (X_{EPAA}), after self-shielding correction ($X_{ss\ corr}$), after γ-ray attenuation correction ($X_{GA\ corr}$) 59

Table 5-6 Comparison *of measured REE concentrations (X_{lab}) with the certified values (X_{cert}) at different steps of* k_0-NAA: concentration obtained from EPAA (X_{EPAA}), after self-shielding correction ($X_{ss\ corr}$), after γ-ray attenuation correction ($X_{GA\ corr}$).....61

Table 5-7 Uncertainty components for the determination of REE-2 by k_0-NAA 62

Table 6-1 Elemental analysis of fresh ore for different particle size (μm) measured with k_0-NAA at SLOWPOKE 66

Table 6-2 Elemental analysis of concentrated ore measured with k_0-NAA at SLOWPOKE 67

Table 6-3 Elemental analysis of selected samples from flotation process with k_0-NAA at SLOWPOKE 68

Table 6-4 Metal content considering the k_0-NAA result and the mass of the samples.....69

Table 6-5 Comparison of REE concentrations measured with k_0-NAA (X_{lab}) with respect to certified values (X_{cer}) for Estuarine sediment, BCR-667 70

LIST OF FIGURES

Figure 1-1 The lanthanide contraction 2

Figure 2-1 Scheme for n, γ 9

Figure 2-2 Decay process of radioactive ^{140}La to stable ^{140}Ce.....10

Figure 2-3 Relation between neutron cross section and neutron energy for ^{103}Rh (n, γ).....12

Figure 2-4 Schematic representation of a typical neutron flux spectrum in a nuclear fission reactor.....14

Figure 2-5 Fission reaction.....23

Figure 2-6 Cumulative chain yield for the fission of ^{235}U as a function of mass number 24

Figure 2-7 Compton effect for NaI detector vs. Ge(Li) detector 27

Figure 3-1 Gamma-ray attenuation 34

Figure 3-2 Exponential attenuation for three different gamma-ray energies 35

LIST OF SYMBOLS AND ABBREVIATIONS

Latin alphabet

Symbol	Definition	Unit
A	Activity	Bq
a (sub)	Analyte	
A(sup)	Nucleon number	
A_{sp}	Specific activity	Bq kg^{-1}
C	Correction for decay during counting	
c	Concentration	mg kg^{-1}
C (sub)	Comparator	
COI	Coincidence summing correction factor	
D	Decay correction	
E	Neutron energy	eV
e (sub)	Epithermal	
E_0	Maxwellian neutron energy (0.025 eV)	eV
E_{Cd}	Effective Cd cut-off energy (0.55 eV in 1 mm Cd)	eV
E_{max}	Maximum energy of epithermal neutrons	eV
E_n	E_n number	eV

$E_{r,i}$	Resonance energy	eV
f	Thermal to epithermal neutron flux ratio	
$g(T_n)$	Westcott's g-factor	
G_e	Correction factor for epithermal neutron self-shielding	
G_{th}	Correction factor for thermal neutron self-shielding	
I_0	Resonance integral for *1/E* epithermal spectrum	b
k_B	Boltzmann constant	eV K^{-1}
M	Molar mass	kg mol^{-1}
m (sub)	Monitor (Not in t_m, where it denotes 'measurement')	
N	Number of radioactive nuclei	
$n(v)$	Neutron density per unit of velocity at neutron velocity v	
N_0	Number of target nuclei	
N_A	Avogadro number	
Q_0	Ratio resonance integral ($1/E$) to 2200 m s^{-1} cross section	
$Q_0(\alpha)$	Ratio resonance integral ($1/E^{1+\alpha}$) to 2200 m s^{-1} cross section	
t_d	Decay time	s
t_{ir}	Irradiation time	s
T_n	Neutron temperature	K
v	Neutron velocity	m s^{-1}

v_0	Neutron velocity at temperature of 293.59 K	m s^{-1}
w	Mass of the sample	g
y_i	Fission yield of the radio-nuclide	

Greek alphabet

Φ_e	Epithermal neutron flux per energy unit	cm^{-2} s^{-1} eV^{-1}
Φ_f	Fast neutron flux per energy unit	cm^{-2} s^{-1} eV^{-1}
Φ_{th}	Thermal neutron flux	$cm^{-2}s^{-1}$ eV^{-1}
φ_e	Epithermal neutron flux	cm^{-2} s^{-1}
φ_f	Fast neutron flux	cm^{-2} s^{-1}
φ_{th}	Thermal neutron flux	cm^{-2} s^{-1}
α	Epithermal neutron flux shape factor	
γ	Gamma-ray abundance (emission probability)	
ε_d	Detection efficiency at distance *d*	
θ	Isotopic abundance	
λ	Decay constant	s^{-1}
σ	Thermal neutron activation cross-section	*b*
μ_x	linear attenuation coefficient	

Abbreviation

ADC	Digital Converter
CRM	Certified reference material
HPGe	High purity germanium
HREE	Heavy rare earth elements
ICP-AES	Inductively coupled plasma atomic emission spectroscopy
ICP-MS	Inductively coupled plasma mass spectrometry
ICP-OES	Inductively coupled plasma optical emission spectrometry
INAA	Instrumental neutron activation analysis
IRMM	Institute for Reference Materials and Measurements
IUPAC	International Union of Pure and Applied Chemistry
LREE	Light rare earth elements
MCA	Multi- Channel Analyzer
MIP-AES	Microwave plasma-atomic emission spectrometer
NAA	Neutron activation analysis
PGNAA	Prompt Gamma Neutron Activation Analysis
REE	Rare earth elements
REO	Rare earth oxide
RNAA	Radiochemical Neutron Activation Analysis

XRF X-ray fluorescence

CHAPTER 1 INTRODUCTION

1.1 Context

1.1.1 Rare earth elements

"These elements perplex us in our searches, baffle us in our speculations, and haunt us in our very dreams. They stretch like an unknown sea before us—mocking, mystifying, and murmuring strange revelations and possibilities"

Sir William Crookes, February 16, 1887

"Rare earths: neither rare, nor earths."

BBC World Service, March 23, 2014

Rare earth elements (REEs) are the fifteen lanthanide series plus yttrium and scandium according to International Union of Pure and Applied Chemistry (IUPAC) [1]. These elements are split into two groups; From La to Eu are referred to as light rare earth elements (LREEs) and heavy rare elements (HREEs) include the remaining lanthanide series from Gd to Lu plus yttrium. Scandium is not included in either the light or the heavy ones [2].

Generally, the ionic radii of elements in periodic table increases with increasing the atomic number. However, this rule does not apply to the rare earth elements and their ionic radii decreases with increasing the atomic number which is referred to as lanthanide contraction [3].

This can be explained by the fact that as the atomic number increases, the increasing positive charge on the nucleus will cause the electron shell of these elements to draw closer to the nucleus while the effect of an added electron is shielded since it is filling the inner 4f sub-shell [4].

Ionic radii of rare earth elements are shown in Figure **1-1**. Their similarity in ionic radii is the explanation for their interchangeability and the difficulty to separate them in most minerals. It also explains why yttrium is considered as one of the heavy rare earth elements (similar ionic

radius and chemical properties) and scandium, with a smaller ionic radius, is excluded from the categories [3].

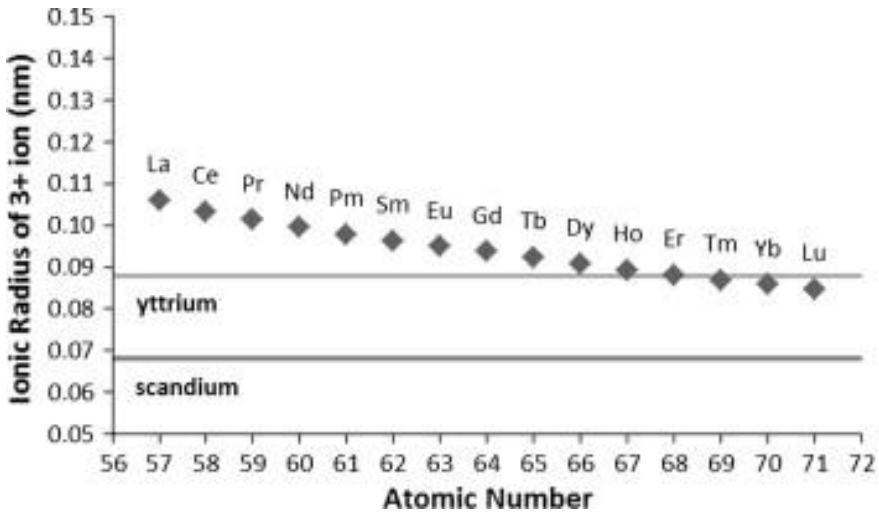

Figure 1-1 The lanthanide contraction (taken from [5])

Contrary to their name, rare earth elements are more abundant in the Earth's crust than commonly exploited elements including platinum group and mercury [2]. Only promethium does not exist naturally. However, the rare earth elements are commonly found in very low concentrations. They are mostly in forms of oxides, silicates, carbonates, phosphates and halides instead of pure metals [5]. There more than 250 kind of minerals discovered that contains rare earth elements with concentrations as low as 10 mg kg^{-1} in some cases [6]. The most important rare earth bearing minerals that are exploited commercially are bastnäsite and monazite with an average rare earth oxide (REO) content of 75 and 61 percent, respectively [7].

The global demand for rare earth elements has increased in recent years due to their growing applications in numerous technologies such as electronic displays, permanent magnets and renewable energy. Table **1-1** illustrates some of the end uses of rare earth elements.

Table 1-1 Selected end-uses of rare earth elements, (adapted from [8])

Light rare earth (more abundant)	Major end-use	Heavy rare earth (less abundant)	Major end-use
Lanthanum	hybrid engines metal alloys	Terbium	permanent magnets phosphors
Cerium	auto catalyst petroleum refining	Dysprosium	hybrid engine permanent magnets
Praseodymium	magnets	Erbium	phosphors
Neodymium	auto catalyst headphones hybrid engines	Yttrium	red colour, ceramics metal alloy agent florescent lamps
Samarium	magnets	Holmium	glass colouring, lasers
Europium	red colour for television and computer screens	Thulium	medical x-ray units
		Lutetium	petroleum refining catalysts
		Ytterbium	lasers, steel alloys
		Gadolinium	Magnets

There are currently 110 million tons of proven REE reserves in the world. Half of these reserves are located in China. Russia and United States are next in line with 17 and 12 percent of the reserves, respectively. There are sizeable deposits in Brazil, India, Australia, Canada and Greenland. However, China still leads in the production of the REE minerals, concentrates and metals with 86 percent in 2012 [7]. The decrease of Chinese exports in 2010 triggered serious concern among REE users. So there is a growing interest in exploiting the reserves in the west.

Metallurgical processes for the extraction of these elements have become widespread. The pathway includes exploitation, mining and refining. Accurate quantification is also critical for any process and development in this field. Therefore, at each step, it is required to monitor REEs recovery by determining their concentration.

1.1.2 Analytical techniques

Quantification of REEs is a challenging task due to their similar physical and chemical properties along with generally low amount and tendency to come together. Increasing demand of more reliable and precise data for REE refining process, monitoring and optimization triggered several research studies. The drawbacks, limitations and uncertainties associated with each REE quantification method were analysed, aiming for higher accuracy of existing analytical techniques while eliminating sources of errors.

Few instrumental methods, such as ICP-OES, ICP-MS, XRD and NAA were able to determine REE with sufficient trueness and precision. Several analyses and comparisons were completed to investigate the capability of ICP-OES, ICP-MS, XRF, RNAA and INAA for determination of REEs [9-13].

1.1.2.1 Plasma-based instrumentation

An ICP-MS combines inductively coupled plasma with a mass spectrometer. The atoms are converted to ions by ICP and then separated by their mass to charge ratio and then detected in the mass spectrometer. It is suggested that the samples have no more than 0.2% wt. total dissolved solids (TDS) in order to avoid blockage in the orifices in the cones. Accordingly, ore and mineral samples needs to be diluted before the analysis. So digestion and dissolution processes needed

prior to the analysis can cause bias in the results. Moreover, REEs analysis can be affected by a possible overlap of M^+, MO^+ or MOH^+ ions of Ba isotopes and oxide ions of lanthanides [9, 11].

Several studies has been done to investigate the compatibility of different types of digestion methods in ICP-MS/MS in comparison with other plasma-based instrumentation including MIP-AES and ICP-AES [11, 14]. They illustrated that MIP-AES is as accurate as ICP-AES, however, in terms of detection limits, ICP-AES has shown better results for the heavy REE. ICP-MS also showed low detection limits although it has to be performed with preliminary interference removal processes to obtain satisfactory results. The use of MS/MS mode, improves detection limits along with minimizing the presence of polyatomic interferences [14].

1.1.2.2 Neutron activation analysis

Another analytical method used to determine rare earth element concentrations is neutron activation analysis which is referred to as a primary method. NAA relies on excitation by neutrons so that the treated sample emits gamma-rays.

Unlike plasma-based methods, neutron activation analysis does not require chemical pre-treatment of the samples and is suitable for characterization of complex solid samples. Especially k_0-NAA, which is a single-comparator standardization method. The advantage of using k_0-NAA over the relative method is its capability to perform multi-elemental analysis with high precision and accuracy without the need to analyse standards.

However, in most of the recent studies [15-18], k_0-NAA application was reported for a limited number of REE, namely, La, Ce, Nd, Sm, Eu, Tb, Yb, Lu, while it can be enhanced to be applicable for accurate determination of most of the rare earth elements at the major, minor and trace levels. As reported in the literature, k_0-NAA for REE requires long cooling times for reducing spectral interferences, while industrial applications are demanding high accuracy and precision with fast turnaround times.

1.2 Objective

The main objective of this research project is to investigate the capability of k_0-NAA for accurate determination of rare earth elements in mineral matrices with short turnaround times. Several sources of systematic error or uncertainty are investigated.

1.3 Plan of the dissertation

This master's dissertation is divided in seven chapters. Chapter 2 presents in detail neutron activation analysis equations, the k_0 method and the latter's fundamental equations. Chapter 3 explains specific objectives and the methodological approach that was adopted with the aim to achieve the main objective of the project. Chapter 4 describes experimental and analytical procedures along with the facilities implemented in this study. Chapter 5 presents a summary of the main results of this work in the form of a scientific article most recently submitted for publication in a scientific journal. A brief summary of the analysis provided for different REE separation processes are presented in Chapter 6. General conclusion and the future recommendation are presented in Chapter 7.

CHAPTER 2 LITERATURE REVIEW AND THEORETICAL ASPECTS OF NEUTRON ACTIVATION ANALYSIS

2.1 Introduction

Following the discovery of neutrons by James Chadwick in 1932, neutron activation analysis was proposed for the first time in Copenhagen, Denmark by George Hevesy and Hilde Levi in 1936. By using (^{226}Ra+Be) as a neutron source and an ionization chamber as a detector, they demonstrated that Dy (Dysprosium) content can be determined through measuring the artificial radioactivity [19, 20]. The development of nuclear reactors in the 40's, the advent of semiconductor detectors in the 60's along with the development of computers and relevant software has improved NAA as a reliable and effective analytical method.

This method is based on measuring the gamma-rays emitted by an excited nucleus which were involved in a neutron capture reaction. The gamma-rays are characteristic for each radio isotope. NAA can be applied in several scientific fields, namely in the cement and coal industries, medicine, biology, anthropology, geology, environmental sciences, industrial elemental analysis, quality control and trace analysis in life sciences [21].

The advantages and drawbacks of NAA can be summarized as follows:

2.1.1 Advantages of neutron activation analysis

- It can be applied to different types of samples
- Detection limits can be as low as 10^{-6} mg kg^{-1}
- It benefits from minimum sample preparation
- Non-destructive analysis
- It is based on nuclear principles unlike most of the chemical methods which are based on the electron's nature.

2.1.2 Drawbacks of neutron activation analysis

- The need for a neutron source
- Working with radioactive materials and the need to handle nuclear waste

- The feasibility of determining of traces of some important elements, such as oxygen, hydrogen and lead is limited. They do not form radionuclides with suitable properties
- Working with liquid samples can be challenging since there is a possibility of leakage during the irradiation and counting processes. This can cause uncertainty associated with the mass of the sample and can create radioprotection issues
- The duration of the analysis can be long for isotopes with long half-lives which makes it less appropriate for industrial applications

2.1.3 Principles of neutron activation analysis

The first step in neutron activation analysis is to convert stable nuclei into radioactive nuclei by bombarding them with neutrons. Radioactive decay takes place by emitting radiation that can be used for analytical purposes. During irradiation, depending on the energy of the neutron, each atomic nucleus can go through one of the following nuclear reactions:

- Transmutation

When the target nucleus captures a neutron and emits particles including alpha, proton, 2 neutrons and deuteron. If the product is unstable, it usually de-excites through a β− decay, e.g.:

$$^{55}_{25}Mn_{30}(n,p)^{55}_{24}Cr_{30}$$

$$^{55}_{24}Cr_{30} \xrightarrow{\beta^-} {}^{55}_{25}Mn_{30}$$

- Fission reaction

Fissionable nucleus (usually Z>90) absorbs a neutron and then splits into two large segments, producing 2 or 3 neutrons. A fission reaction can become a chain reaction and be a source of neutrons.

- Inelastic scattering

In this case, the neutron is not captured by the target nucleus and only part of its energy is transferred to the neutron.

- Neutron capture

The target nucleus collides with a neutron resulting in a product isotope, in this process the mass number increases by one. The product will instantaneously de-excite into a more stable configuration through the emission of the prompt gamma-rays. In most cases, the compound nucleus is also unstable and decays through the emission of a beta particle with a distinctive half-life. Prompt gamma-rays can be measured to determine elements such as H, B, C, N, P, S, Cd and specifically Sm and Gd. Most of the light elements cannot be determined with NAA, therefore prompt gamma neutron activation analysis (PGNAA) can be complementary method. These processes are shown in Figure **2-1**.

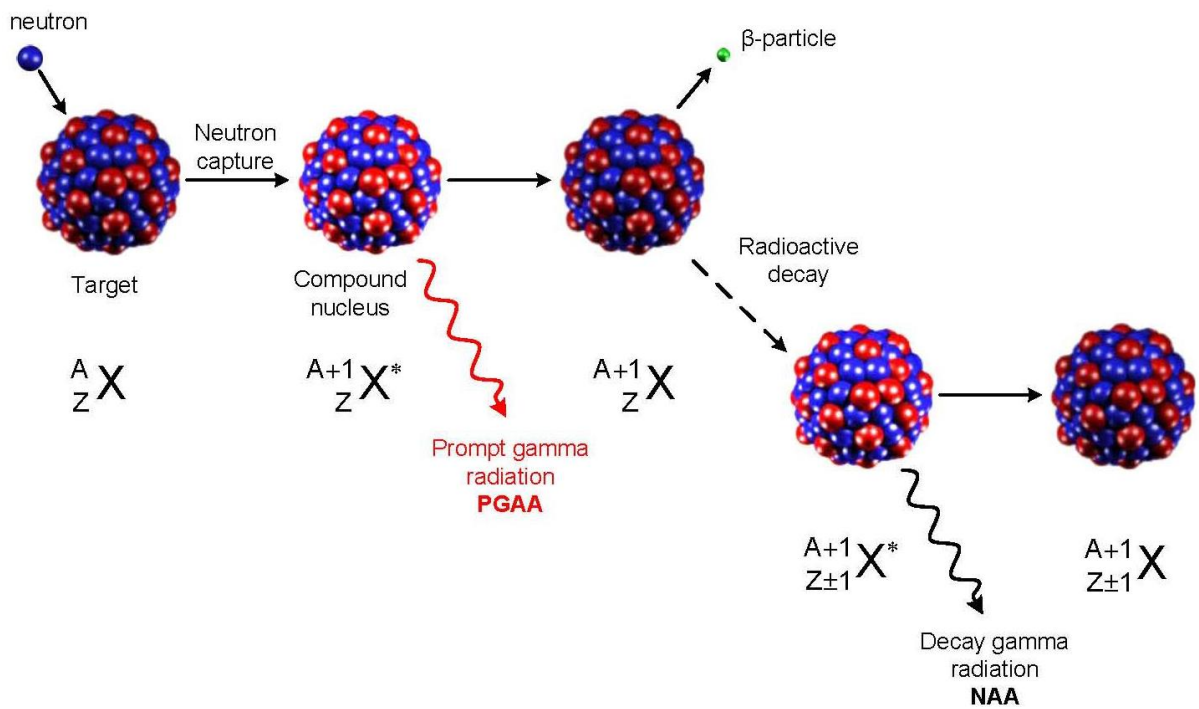

Figure 2-1 Scheme for (n,γ), (taken from [22])

The neutron capture for lanthanum as the target nucleus is illustrated as:

$$^{139}_{57}La + ^{1}n \rightarrow ^{140}_{57}La + (prompt)\gamma - radiation$$

Which also can be presented as below:

$$^{139}_{57}La(n,\gamma)^{140}_{57}La$$

The (n,γ) reaction is a fundamental reaction for neutron activation analysis.

By absorbing a neutron, ^{139}La is converted to ^{140}La with emission of a prompt gamma. ^{140}La is an unstable nuclide with a half-life of 40.27 h which emits a beta and transforms to ^{140}Ce. Figure **2-2** elaborates the decay process of ^{140} La to ^{140}Ce.

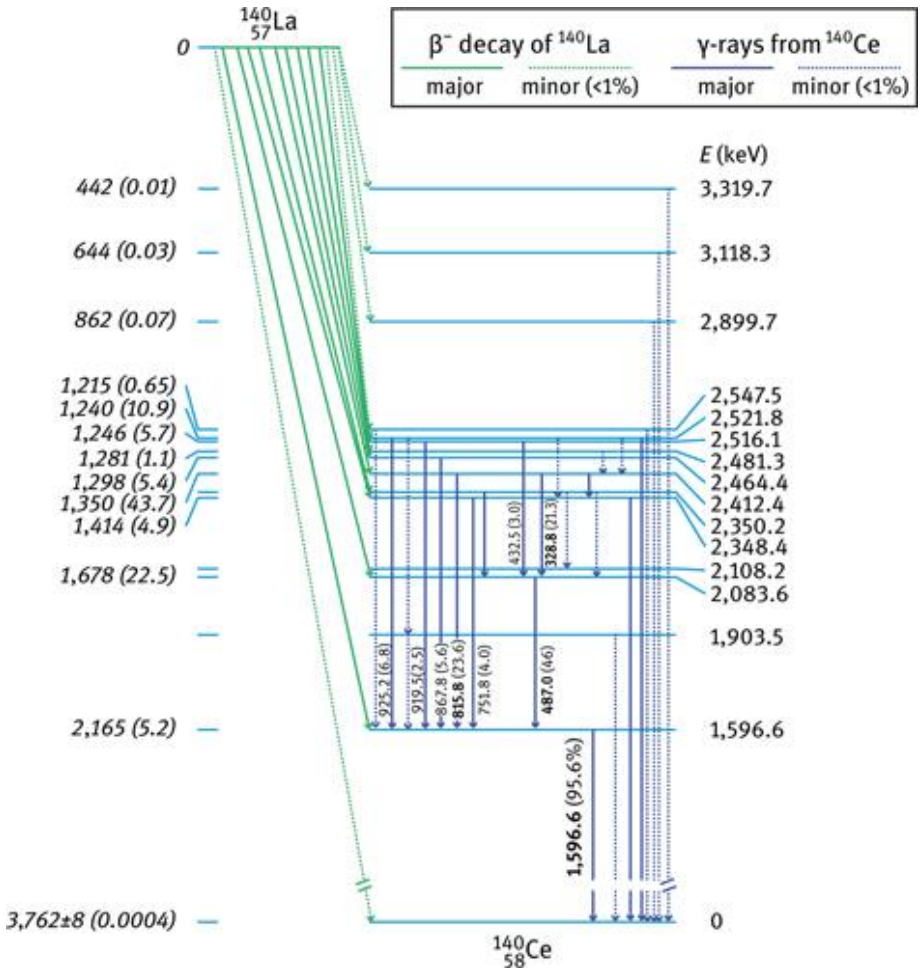

Figure 2-2 Decay process of radioactive ^{140}La to stable ^{140}Ce, (taken from [23])

2.1.3.1 Neutron cross section

The probability of a neutron undergoing a nuclear reaction with a nucleus is dependent on the energy of the neutron. This probability is referred to as a neutron cross section. The larger the cross section, the more probable it is that the neutron will have a reaction with the nucleus. The standard unit for measuring the cross section is the barn (b) = 10^{-24} cm^2.

2.1.3.2 Reactor neutron spectrum

Neutrons are classified according to their kinetic energy as follows:

2.1.3.2.1 Thermal neutrons (0.025 eV – 0.55 eV)

Neutrons in thermal equilibrium with a surrounding medium are called thermal neutrons. Applying the relation $E = k_B \times T$, (k_B is Boltzmann's constant= 8.617×10^{-5} eV K^{-1}), we can calculate that the most probable energy at 300 K corresponds to an energy of 0.026 eV. Thermal neutrons constitute the most important part of the neutron spectrum in thermal reactors [23].

2.1.3.2.2 Epithermal neutrons (0.55 eV-100 eV)

Fast neutrons that are slowed down by a collision with the surrounding material are called epithermal neutrons.

2.1.3.2.3 Fast neutrons (100 keV-25 MeV)

Neutrons with kinetic energy greater than 1 MeV are called fast or fission neutrons. The main source of these neutrons are nuclear fission reactions. The mean energy for these neutrons are 2 MeV (^{235}U fission). The fission neutrons are thermalized inside the reactor through neutron moderation [22].

In most of the cases, the cross section has a $1/v$ behaviour in the thermal region and has resonances in the epithermal region. The $1/v$ behaviour in the thermal regions leads to an activation independent of the neutron temperature and neutron density energy distribution. Normally the $1/v$ cross section can be described as $\sigma(v) = \sigma(v_0)\, v_0/v$ where v_0 is 2200 m s^{-1} which is the velocity of neutrons at a temperature of 293.59 K. The non $1/v$ nuclides show resonance in the thermal region [24].

Neutron cross section (σ) dependence on the neutron energy for ^{103}Rh is elaborated in Figure **2-3**. For thermal neutrons, σ decreases approximately as a function of $1/v$. The epithermal range is characterized by a resonances defined as "*the sharp increases in σ at well-defined energies which is related to resonances, the formation of a compound nucleus in discrete excited states*"[23]. ^{103}Rh has a sharp resonance at energy of 1.26 eV.

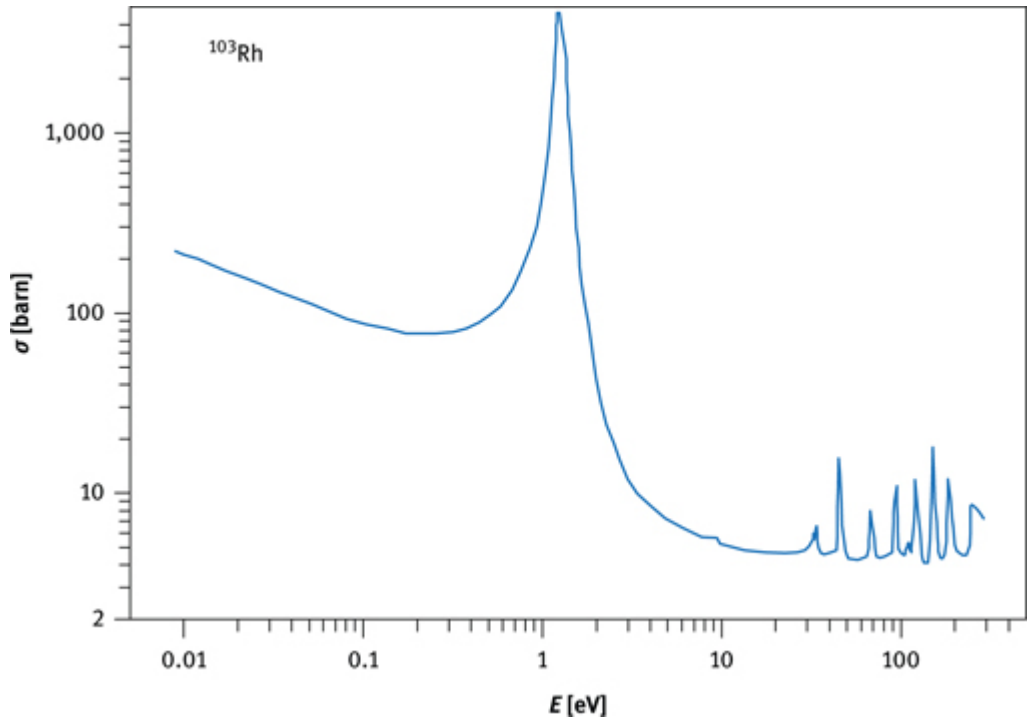

Figure 2-3 Relation between the neutron cross section and neutron energy for ^{103}Rh (n, γ), (taken from [1])

2.1.3.3 Neutron flux

The amount of neutrons available for irradiation in the nuclear reactor is described by the neutron flux. In other words, the neutron flux is the number of incident neutrons per square centimeter per second, and cm^{-2} sec^{-1} is the unit used for measuring the neutron flux. The neutron energy spectrum in the nuclear reactor can be represented as follows [25]:

$$\varphi(E) = \varphi_f(E) + \varphi_e(E) + \varphi_{th}(E) \quad (2\text{-}1)$$

$$= 0.484\ \Phi_f e^{-E} \sinh(\sqrt{2.E}) \quad \text{(E>10 keV)} \quad (2\text{-}2)$$

$$+ \frac{\Phi_e(E)}{E^{1+\alpha}} [\left(1 - \exp\left(-\frac{E^2}{E_c^2}\right)\right) \exp(-\frac{E}{E_d})] \quad \text{(0.1 eV<E< 100 keV)} \quad (2\text{-}3)$$

$$+ \Phi_{th} \frac{E}{E_0^2} \exp(-\frac{E}{E_0}) \quad \text{(E<1 eV)} \quad (2\text{-}4)$$

Where

φ_f , Φ_f fast neutron flux per unit energy, total fast neutron flux

φ_e, Φ_e epithermal neutron flux per unit energy, total epithermal neutron flux

φ_{th}, Φ_{th} thermal neutron flux per unit energy, total thermal neutron flux

E_c=0.1 eV, E_d=300 keV and $E_0 = k\,T_n$ (=0.0253 eV at 20°C) [25].

The fission process in the reactor produces fast neutrons and the energy distribution for these neutrons can be presented by the Watt distribution in equation (2-2). Moreover, the behavior of thermal neutrons is described by the Maxwell-Boltzmann distribution in equation (2-4). In the presence of moderators, the fast neutrons can be slowed down to the epithermal region. Equation (2-3) describes the behaviour of the epithermal neutrons [25]. The α in the term $1/E^{1+\alpha}$ shows how much the epithermal fluence rate deviates from the 1/*E* behaviour in real irradiation sites. Closer to the core of the reactor, the number of epithermal neutrons are higher compared to thermal neutrons. Also, the spectrum is closer to the 1/*E* form (α closer to zero) and as one gets farther away from the core, the epithermal flux deviates from its 1/*E* behaviour. In order to illustrate these features, a typical distribution of the neutron flux in a nuclear reactor is presented in Figure **2-4**.

Thermal neutron activation analysis requires at least a minimum neutron flux of 10^9 cm^{-2} sec^{-1}. As indicated in Figure **2-4**, the highest flux component is related to thermal neutrons. Epithermal and fast neutrons are dependent on the active core of the reactor and also on the effectiveness of the moderator.

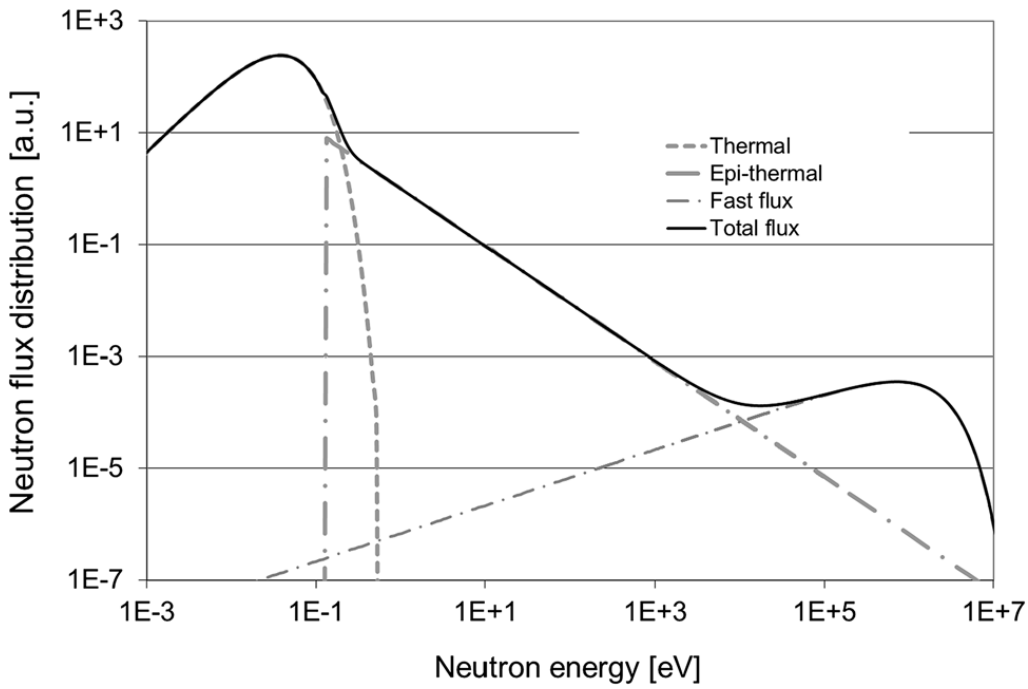

Figure 2-4 Schematic representation of a typical neutron flux spectrum in a nuclear fission reactor, (taken from [24])

2.1.3.4 Activation

The number of nuclide decaying per unit of time is called activity (*A*). The probability for a nucleus to decay per unit of time is referred to decay constant (λ). Therefore, the activity can be expressed as

$$A = N\lambda \tag{2-5}$$

Reaction rate (*R*) of neutron capture reaction is defined by the following:

$$R = \int_0^{\infty} n(v).v.\sigma(v).dv \tag{2-6}$$

Where

$n(v)$ neutron density per unit of velocity at neutron velocity *v*

$\sigma(v)$ cross section

Production of radioactive nuclei can be described by equation (2-7).

$$\frac{dN}{dt} = R.N_0 - \lambda.N \tag{2-7}$$

Where

N_0 number of target nuclei

N number of radioactive nuclei

λ decay constant in s^{-1}

For an irradiation time of t_i, the disintegration rate of the produced radionuclide can be calculated from the following equation:

$$A(t_i) = N(t_i)\lambda = N_0 R(1 - e^{-\lambda t_{ir}}) \tag{2-8}$$

The activation cross section and neutron flux density are dependent on the neutron energy. By dividing the neutron spectrum into thermal and epithermal components in equation (2-6), we can obtain:

$$R = \int_0^{v_{Cd}} n(v).v.\sigma(v)dv + \int_{v_{cd}}^{\infty} n(v).v.\sigma(v)dv \tag{2-9}$$

This approach is known as Høgdahl convention.

The division is made at the Cd cut off energy. ^{113}Cd specific absorption cross-section is significant for neutrons with kinetic energies less than 0.55 eV, also referred to as cadmium cut-off energy. Consequently cadmium is widely used as thermal neutron filters [25].

The thermal part can be calculated directly

$$\int_0^{v_{Cd}} n(v)\, v\, \sigma(v)dv = v_0\, \sigma_0 \int_0^{\infty} n(v)dv = v_0\, \sigma_0 n \tag{2-10}$$

Where $n = \int_0^{\infty} n(v)dv$

The epithermal portion can be transformed more conveniently when integrating according to energy. So the infinite dilution resonance integral, I_0 can be calculated as

$$\int_{v_{cd}}^{\infty} n(v)\, dv = \emptyset_e \int_{E_{Cd}}^{E_{max}} \frac{\sigma(E) dE}{E} = \emptyset_e\, I_0 \tag{2-11}$$

It can be seen from the definition of I_0 that the epithermal neutron flux density is proportional to *1/E*.

As explained in section 2.1.3.3, in real reactors a new parameter is needed to describe the epithermal neutron density. This parameter can be measured and is introduced by:

$$I_0(\alpha) = \int_{E_{Cd}}^{E_{max}} \frac{\sigma(E) dE}{E^{1+\alpha}} \tag{2-12}$$

The reaction rate can be rewritten as:

$$R = \emptyset_{th}\, \sigma_0 + \emptyset_e\, I_0(\alpha) \tag{2-13}$$

After applying the correction on self-shielding, we obtain:

$$R = G_{th}\, \emptyset_{th}\, \sigma_0 + G_e\, \emptyset_e\, I_0(\alpha) \tag{2-14}$$

The ratio of the thermal and epithermal neutron fluxes can be expressed as *f*:

$$f = \frac{\emptyset_{th}}{\emptyset_e} \tag{2-15}$$

Also Q_0 is referred to as the epithermal to thermal cross section

$$Q_0(\alpha) = \frac{I_0(\alpha)}{\sigma_0} \tag{2-16}$$

In addition, the effective cross-section can be introduced as

$$\sigma_{ef} = \sigma_0(1 + \frac{Q_0(\alpha)}{f}) \tag{2-17}$$

So equation (2-13) simplifies to $R = \emptyset_{th}\sigma_{ef}$.

Nuclear transformations are represented by measuring the number of nuclear decays. That being said, the number of activated nuclei present at the start of the measurement can be calculated from equation (2-18)

$$N(t_{ir}, t_d) = \frac{RN_0}{\lambda}\left(1 - e^{-\lambda.t_{ir}}\right)e^{-\lambda.t_d} \tag{2-18}$$

Where t_{ir}, t_d are the irradiation and decay time, respectively. Moreover, the number of nuclides disintegrating during the measurement can be calculated through equation (2-19).

$$N(t_{ir}, t_d, t_m) = RN_0\left(1 - e^{-\lambda t_{ir}}\right)e^{-\lambda.t_d}\frac{(1 - e^{\lambda t_m})}{\lambda t_m} = RN_0SDC \tag{2-19}$$

Therefore, by measuring the emitted gamma-rays and considering the half-life, the radio nuclides can be identified and quantified. By introducing (θ), the isotopic abundance and mass of the sample, *w*, the parameter N_0 can be rewritten as $(N_{Av}\theta\frac{w}{M})$

By using $R = \emptyset_{th}\sigma_{ef}$ as the reaction rate and considering the coincidence correction factor COI in net peak area, the activation equation can be written as:

$$\frac{N_p}{COI} = \Delta N\gamma\varepsilon = R\frac{N_A\theta w}{M}SDC\gamma\varepsilon \tag{2-20}$$

Where N_p is number of counts in the full-energy peak when taking to account pulse losses.

As for the (n, γ) reaction, the reaction rate can be represented using the number of impulses in a given peak by

$$R = \frac{\frac{MN_p}{SDC\ COI\ wt_m}}{N_A\theta\varepsilon\gamma} \tag{2-21}$$

As for the epithermal neutrons, the reaction can be introduced as:

$$R_e = \frac{M\left(\frac{N_p}{SDC\ COI\ wt_m}\right)_{Cd}}{N_A \theta \varepsilon \gamma} \tag{2-22}$$

If we define the specific activity as: $A_{sp} = N_p/\gamma\varepsilon\ COI$.

Reaction rate for thermal neutrons can be rewritten as

$$A_{sp} = \frac{N_p}{SDC\ COI\ wt_m} \tag{2-23}$$

By combing equation (2-23) and equation (2-14), one finds:

$$A_{sp} = \frac{N_A \theta \gamma}{M}\left[G_{th}\ \phi_{th}\ \sigma_0 + G_e\ \phi_e\ I_0(\alpha)\right]\varepsilon \tag{2-24}$$

2.2 Methods of standardization

So the concentration of the nuclide can be derived from the following equation:

$$c_a = \frac{M_a w_a}{N_A\ \theta_a\ \gamma_a\ w} \cdot \frac{\left(\frac{N_p}{SDC\ COI\ t_m}\right)_a}{\left[G_{th}\ \phi_{th}\ \sigma_{0,a} + G_{e,a}\phi_e I_{0,a}(\alpha)\right]\varepsilon_a} \times 10^6 mg\ kg^{-1} \tag{2-25}$$

There are three types of standardization: absolute, relative and comparator standardization methods. In this context, the use of word ‘standardization’ refers to ‘calibration of NAA’, which consists in finding the relation between the concentration of the analyte and the intensity of the related peak [25]. A review was completed regarding the features and drawbacks of these three methods [26].

2.2.1 Absolute standardization

In this method, the calculation of the concentration is feasible according to the form described in equation (2-25). Also, equation (2-25) can be used when the burn-up effect can be neglected and nuclear values related to the reactor (α, f, ϕ_{th}) are staying constant otherwise it is vital to monitor

the stability of these parameters during the irradiation. In this case, equation (2-25) will be transformed to:

$$c_a = \frac{\left(\frac{N_p}{SDC\ COI\ wt_m}\right)}{wA_{sp,m}} \cdot \frac{M_a \theta_m \gamma_m \sigma_{0,m}}{M_m \theta_a \gamma_a \sigma_{0,a}} \cdot \frac{G_{th,m} f + G_{e,m} Q_{0,m}(\alpha)}{G_{th,a} f + G_{e,m} Q_{0,a}(\alpha)} \cdot \frac{\varepsilon_m}{\varepsilon_a} \cdot 10^6 mg\ kg^{-1} \qquad (2\text{-}26)$$

Although this approach is experimentally simple, the accurate knowledge of nuclear parameters is necessary. Poor knowledge of accurate values can be a source of systematic error up to 20% [25, 27]. In addition, the need for accurate neutron distribution characteristics, accurate detector efficiency and neutron self-shielding factors are also required.

2.2.2 Relative method of standardization

In this method, a chemical standard with a known mass of w_s of an element to be determined needs to be irradiated along with the sample. Both of the samples should be irradiated in the same geometrical conditions with respect to the detector. Since $S_a = S_s, M_a = M_s, \gamma_a = \gamma_s, \sigma_{0,a} = \sigma_{0,s}, I_{0,a} = I_{0,s}, and\ \theta_a = \theta_s$ equation (2-25) can be rewritten for the standard and the sample and combined into equation (2-27):

$$c_a = \frac{\left(\frac{N_p}{DCwt_m}\right)_a}{\left(\frac{N_p}{DCwt_m}\right)_s} \cdot \frac{G_{th,s} f + G_{e,s} Q_{0,s}(\alpha)}{G_{th,a} f + G_{e,a} Q_{0,a}(\alpha)} \cdot \frac{\varepsilon_s}{\varepsilon_a} \cdot 10^6 mg.kg^{-1} \qquad (2\text{-}27)$$

It is assumed that the neutron flux for sample and the standard is constant. The detection efficiency and gamma attenuation in the sample and standard should be taken into account.

For multielement analysis, this technique has several disadvantages:

- The preparation of standards can be time consuming
- In some situations the detection of element is not possible if the standards for that element is not available

- Homemade multi-element standards need to be prepared with a high chemical stability for the components and with high homogeneity

It should be noted that the certified reference materials (CRM) and commercial multielemental reference materials should be used only for quality control purposes since the uncertainty of the elements' concentrations is usually higher than in-house standards. In addition, CRMs are costly and are available in limited quantities [27, 28].

2.2.3 Comparator method of standardization

The single-comparator standardization method applies *k*-factors. These values are determined experimentally by co-irradiating the standard with a single comparator together.

$$k_c(s) = \frac{A_{sp,s}}{A_{sp,c}} \tag{2-28}$$

$k_c(s)$ in equation (2-28) is defined as:

$$k_c(s) = \frac{M_c.\theta_s\gamma_s\sigma_{0,s}}{M_s.\theta_c\gamma_c\sigma_{0,c}}.\frac{G_{th,s}.f + G_{e,s}.Q_{0,s}(\alpha)}{G_{th,c}.f + G_{e,c}.Q_{0,c}(\alpha)}.\frac{\varepsilon_s}{\varepsilon_c} \tag{2-29}$$

If the following conditions are met, the concentration can be calculated from equation (2-30), thus:

- There should be no significant deviation between the irradiation conditions (f, α) in the case of the analysis and the determination of $k_c(s)$
- $\theta_a = \theta_s$
- Neutron self-shielding should also be similar in both analyte-comparator and standard-comparator, the best case is to make G_{th}=G_e=1 in order to find:

$$c_a = \frac{\left(\frac{N_p}{S.D.C.w.t_m}\right)_a}{A_{sp,c}}.\frac{10^6}{k_c(s)} mg.kg^{-1} \tag{2-30}$$

This method offers the same advantages as the absolute method while there is no flux deviation problem. Moreover, by determining precisely the *k* factors values, the flux ratio, and the counting efficiency, the total uncertainty of the measurements can be reduced.

On the other hand, selecting suitable comparator elements for a multi-element analysis can be challenging. Since calibrating the analysis calculations based on all sample-detector geometry positions, corrections of coincidence summing and attenuation can be tedious [27].

2.2.4 k_0-method of standardization

If the *k*-factors in single-comparator method are normalized based on the experimental conditions such as (f,α) for the irradiation stage, (ε) for the counting stage, the following equation will be obtained:

$$k_{0,c}(s) = k_c(s).\frac{G_{th,c}f + G_{e,c}Q_{0,c}(\alpha)}{G_{th,s}f + G_{e,s}Q_{0,s}(\alpha)}.\frac{\varepsilon_{p,c}}{\varepsilon_{p,s}} \tag{2-31}$$

$$= \frac{A_{sp,s}}{A_{sp,c}}.\frac{G_{th,c}f + G_{e,c}Q_{0,c}(\alpha)}{G_{th,s}f + G_{e,s}Q_{0,s}(\alpha)}.\frac{\varepsilon_{p,c}}{\varepsilon_{p,s}} \tag{2-32}$$

So the k_0-factors can be defined as a nuclear constant:

$$k_{0,c}(s) = \frac{M_c.\theta_s.\sigma_{0,s}.\gamma_s}{M_s.\theta_c.\sigma_{0,c}.\gamma_c} \tag{2-33}$$

These values are measured experimentally and published in the literature [29-33]. If the samples are coirradiated with the monitor, where the $k_{0,c(m)}$-factors are available, we have:

$$\frac{k_{0,c}(s)}{k_{0,c}(m)} = k_{0,m}(s) \tag{2-34}$$

So the analyte concentration can be obtained as

$$c_a = \frac{\left(\frac{N_p}{SDC\ COI\ wt_m}\right)}{A_{sp,m}}.\frac{k_{0,c}(m)}{k_{0,c}(a)}.\frac{G_{th,m}f + G_{e,m}Q_{0,m}(\alpha)}{G_{th,a}f + G_{e,a}Q_{0,a}(\alpha)}.\frac{\varepsilon_m}{\varepsilon_a}.10^6 mg\ kg^{-1} \tag{2-35}$$

Respecting the condition that $\theta_a = \theta_s$.

As explained before, all these equations are written in the Høgdahl convention (modified for $1/E^{1+\alpha}$). In this formalism, it is considered that the cross section for all the nuclides follows a $1/v$ behaviour. While this is true for most of the nuclides, there are some exceptions where the deviation is significant: ^{151}Eu(n,γ)^{152m}Eu, ^{151}Eu(n,γ)^{152}Eu, ^{168}Yb(n,γ)^{169}Yb, and ^{176}Lu(n,γ)^{177}Lu.

In these few cases, the Westcott formalism [34] is applicable and the $[f+Q_{0,m}(\alpha)]/[f+Q_{0,a}(\alpha)]$ ratio in equation (2-24) should be replaced by

$$\frac{g_{Au}(T_n) + r(\alpha)\sqrt{T_n/T_0} \times s_{0,Au}(\alpha)}{g_a(T_n) + r(\alpha)\sqrt{T_n/T_0} \times s_{0,a}(\alpha)} \tag{2-36}$$

Where $g(T_n)$ is the 'Westcott's g-factor' and T_n is the neutron temperature, $g(T_n)$ is a factor used to describe the deviation from the $1/v$ behaviour of the thermal radiative cross section, $r(\alpha)\sqrt{T_n/T_0}$ is the spectral index and $s_0(\alpha)$ is the epithermal to thermal cross-section ratio modified for the $1/E^{1+\alpha}$ epithermal spectrum.

2.3 Equipment

2.3.1 Nuclear reactors

Since 1970, different sources have been used for generating neutrons, namely, accelerators, neutron generators, isotopic neutron sources and nuclear reactors. The most important source of neutrons is the nuclear reactor which is based on the fission process of ^{235}U. Thermal neutrons have high cross section of 586 b for this process. Fission of ^{235}U produces 2 to 3 neutrons together with two large fission fragments. The fission reaction can be expanded by the equation (2-37).

$$^{235}_{92}U + ^{1}_{0}n \rightarrow ^{A_1}_{Z_1}X + ^{A_2}_{Z_2}Y + v^{1}_{0}n \tag{2-37}$$

Figure **2-5** shows fission process of ^{235}U.

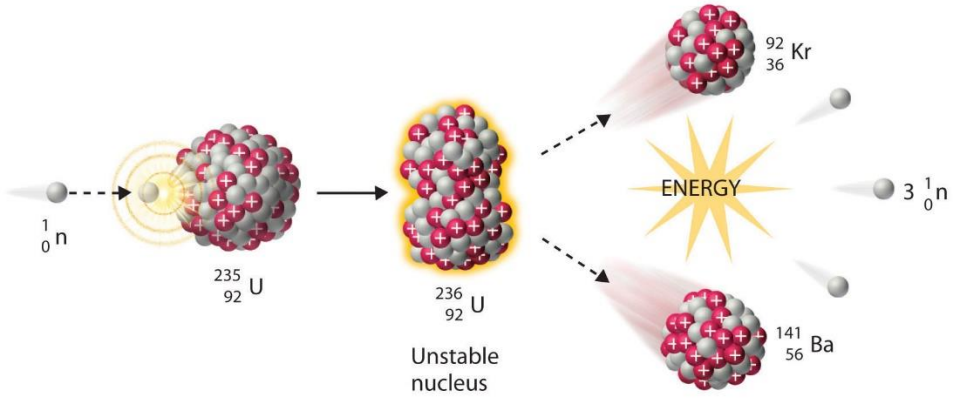

Figure 2-5 Fission reaction (taken from [22])

The 2 to 3 neutrons generated through fission of uranium are fast neutrons which need to be thermalized to start another fission reaction. Therefore they have to be thermalized by the moderator. Moderators are usually light elements like hydrogen, carbon and oxygen. The choice of moderators can affect the thermal and epithermal neutron ratio. In nuclear reactors with light water as a moderator, an epithermal neutron flux can be 20-50 times lower than a thermal neutron flux.

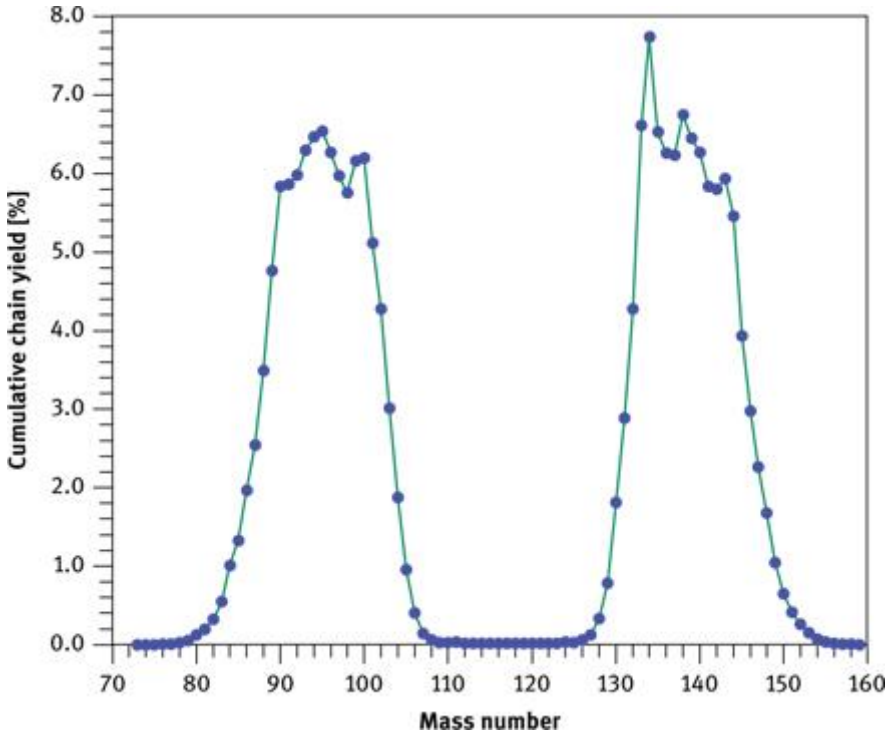

Figure 2-6 Cumulative chain yield for the fission of ^{235}U as a function of mass number (taken from [23])

Figure **2-6** shows the yield of uranium products with respect to the mass number. As interpreted from Figure **2-6**, two large segments produced by uranium fission have masses around 90–100 and 133–143. If the sample that needs to be analysed contains uranium, there will be some light rare earth elements in the sample which are produced by ^{235}U fission. This can be a major source of error in NAA when determining rare earth elements in the samples containing ^{235}U [23, 35].

With the decommissioning of the reactors, there are six research reactors currently remaining in Canada. Research reactors are much smaller than the reactors used in a nuclear power plants. They have been used for research, analytical purposes and production of radioactive substances for medical and industrial uses [36].

2.3.2 The counting system

The gamma-spectroscopy system used is composed of high-purity germanium (HPGe) detectors and pulse-processing electronics. The electronic system consists of a high voltage power supply, amplifier, analogue to digital converter (ADC) and Multi-Channel Analyzer (MCA). Their role can be summarized by collecting the electrons produced by the incident gamma-rays and sorting them by energy. This procedure can be summarized as follows [23, 37]:

- The gamma photons interact with the detector crystal which leads to the production of electrons
- Voltage is applied to sweep electrons from the crystal
- Electrons produced make a current which forms signal pulse
- Preamplifier is required to increase the pulse size
- The amplifiers are used to boost the signal registered in the detector in order to reach a high signal-to-noise ratio
- ADC is used to convert signal intensity to numerical value to be sent to MCA
- MCA sorts the signals as a function of their energy
- The evaluation of the spectra is done by the analyst with a software

2.3.3 Detectors

One of the most important parameters that represents a characteristic of a detector is efficiency. Absolute efficiency can be defined as the observed counts in the detector per unit of time divided by the absolute photon rate emitted by the source. Efficiency depends on sample-detector geometry and the distance between the sample and the detector.

Another concept used in the detection efficiency is relative efficiency which is defined as the relative photopeak efficiency of a detector compared to that of a 3 in. × 3 in. NaI (Tl) detector at an energy of 1333 keV (^{60}Co) and a distance of 25 cm between source and detector.

The relative efficiency increases with the volume of the detector. On the other hand, efficiency decreases with a gamma energy proportional to $E^{-0.5}$ and at energies above about 300 keV. A

typical germanium detector has a maximum efficiency at 100 keV and decreases by about one order of magnitude at 1333 keV.

Another characteristic of the detectors is its resolution defined as its ability to separate the closely spaced peaks. It is reported as FWHM (full width at half maximum) which is the width of a peak at half of its maximum intensity. For planar Ge detectors resolution is reported for the 121.8 keV peak of ^{152}Eu or the 122.1 keV γ-peak of ^{57}Co. For large HPGe detectors, resolution is usually specified for the 1333 keV line of ^{60}Co. Planar Ge detector is better choice for detecting gamma energies below ≈150 keV because 'high-energy gamma rays are much less likely to be absorbed in a planar detector than in a high-volume Ge detector' so the Compton background is reduced [23, 35].

2.3.3.1 Interaction of electromagnetic radiation with matter

The absorption of gamma-rays or X-rays by matter follows equation (2-38)

$$I = I_0 \times \exp(-\mu d) \tag{2-38}$$

Where I_0 is the intensity of the photon before travelling through a distance of *d (cm)* in the matter. The $\mu\ (cm)$is the absorption coefficient which is the sum of three effects including the photoelectric effect, the Compton effect and the pair-production effect.

2.3.3.1.1 Photoelectric effect

In the photoelectric effect, total energy of the photon is transferred to an electron's orbital and in about 80 % of cases leads to a K electron and in 20 % to an L electron. The energy of the electron emitted will be the energy of the photon minus the binding energy of that electron. Immediately, the gap is filled with an electron from the next higher shell, and a characteristic X-ray is emitted accordingly.

2.3.3.1.2 Compton effect

The Compton effect is the result of an elastic scattering between a gamma-ray and an electron, which creates an energetic recoil electron and a scattered gamma-ray photon. Only part of the energy of the photon is transferred to the electron which is dependent on the scattering angle [38].

The scattered photon may be absorbed by the photoelectric effect, undergo more Compton effect or escape from the detector. In case the energy of the photon is absorbed by the detector, it contributes to the Compton continuum, which referred to a region with an undesired high background in a gamma spectrum. As for ^{60}Co with a gamma energy of 1333 keV, by calculating the energy of the electron we get the value of 1119 keV which is called Compton edge, illustrated in Figure **2-7**.

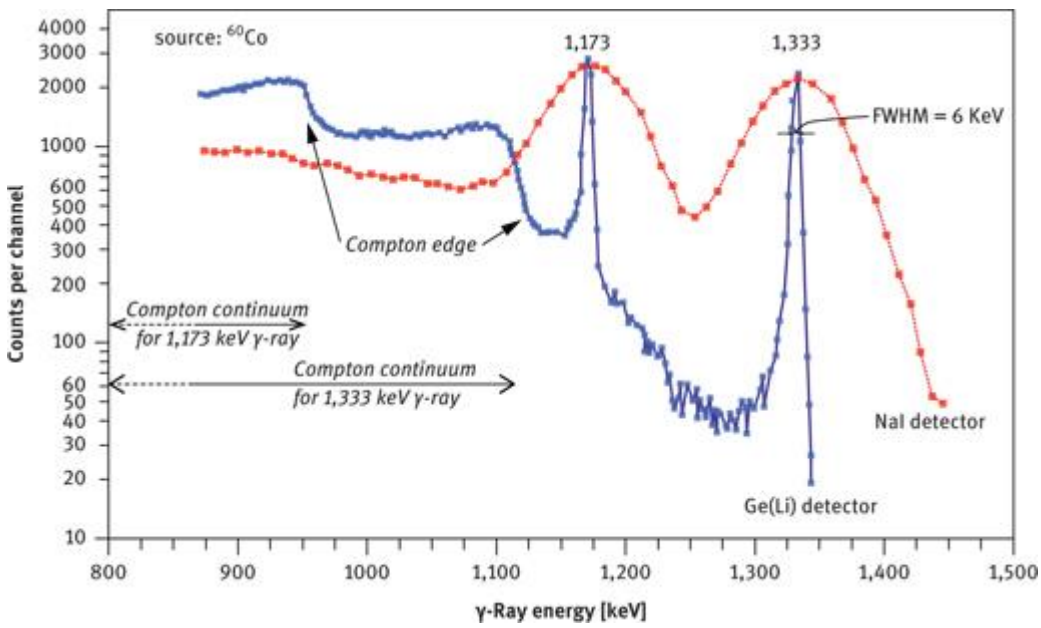

Figure 2-7 Compton effect for NaI detector vs. Ge(Li) detector, (taken from [23])

2.3.3.1.3 Pair-production effect

When the photon is in the strong electromagnetic field near the nuclei of the absorbing material, it may interact with an absorber nucleus and produce an electron-positron pair. This refers to a pair production effect and it occurs at very high energies. The minimum energy of a gamma that can cause pair production is equal to the sum of the rest masses of the electron and positron which is 1022 keV (511 keV each). The remaining part of the energy of the incident photon will turn into a kinetic energy for an electron and positron. When the positron has lost this energy, it annihilates by reacting with another electron and consequently generating two 511 keV γ-rays [23]. These gamma energies can be absorbed to the detector or undergo Compton effect [23, 38].

CHAPTER 3 SPECIFIC OBJECTIVES AND METHODOLOGICAL ASPECTS

Neutron activation analysis has been used for the determination of rare earth elements in geological samples. With the advent of Ge(Li) detectors in 1963, Gordon et al.[39] were able to determine La, Ce, Sm, Eu, Tb, Tm, Tb and Lu in standard rock samples but with cooling times up to a few months. In 1978, Duffield et al. [40] applied a radiochemical separation after the irradiation in order to obtain the concentration of rare earth elements in the rocks. They were able to determine all the 14 rare earth elements with a shorter cooling time of 12 days.

Many studies have been done to determine the REE distribution in rocks, sediments, meteorites using NAA [11, 41-44]. Danko et al. [45] have conducted a study on REE content in biological materials by NAA with pre- and post-irradiation separation. They were able to assess the concentration of 13 REE (excluding Gd) in 4 weeks.

Several studies have been done in order to assess the REE content with k_0-NAA [15-18]. Ravisankar et al. [16] determined the La, Ce, Sm, Eu, Tb, Yb content in beach rock samples with a longer cooling time of 30-50 days. Silachyov et al. [46] compared internal standard method and single comparator method for determining rare earth elements in rock samples. They were able to measure La, Ce, Nd, Sm, Eu, Tb, Yb, Lu with decay time of 7 days and 30 days. Xiao et al. [18] investigated the uranium fission interference on the measurement of Nd, Ce and La and were able to determine La, Ce, Nd, Sm, Eu, Tb, Yb and Lu in ore reference material.

The accurate analysis of REEs in mineral matrices with high contents of REEs in short turnaround times poses several challenges in terms of analytical aspects which can lead to systematic error or uncertainty in the measurements. In the previous works, this has been avoided by radiochemical separation or long cooling times. In this study we have investigated the possible sources that can bring systematic error to the analysis, with the aim of reducing the turnaround time while conserving the accuracy.

3.1 Sources of error

First objective of this study is to verify the validity and the efficiency of the libraries used at Polytechnique Montreal for determination of rare earth elements.

3.1.1 Nuclear data, detection efficiency

Ecole Polytechnique Activation Analysis (EPAA) software is used as part of the k_0-NAA analysis at SLOWPOKE laboratory. The libraries associated with this software are generated based on the k_0 method and detection efficiency model which can be summarized in the sensitivity factors (B) [47].

$$B = \frac{N_{Av}\theta_{Au}\sigma_{0,Au}I_{Au}}{M_{Au}} k_0(1 + \frac{Q_0(\alpha)}{f})\varepsilon \tag{3-1}$$

Where

N_A	Avogadro number
θ_{Au}	Au isotopic abundance
$\sigma_{0,Au}$	Au radiative cross section at 2200 m.s^{-1}
I_{Au}	Au 411.8 keV gamma-ray intensity
M_{Au}	Au atomic mass
$Q_0(\alpha)$	resonance integral ($1/E^{l+\alpha}$) to 2200 m.s^{-1} cross-section ratio
f	ratio of thermal to epithermal flux
ε	peak relative detection efficiency

The accuracy of k_0-NAA depends on the method's core parameters which are k_0 and Q_0 factors. Since introducing the first generation of k_0 values [28, 48-51], each decade an updated version is published but there are still some values that have not been re-determined since 30 years ago. There have been several studies at Polytechnique Montreal in order to verify these values [32, 33] yet not all of the rare earth elements are among the re-measured values.

Along with the k_0 standardization method, the efficiency model is included in the library data, thus:

$$\varepsilon = \varepsilon_{250mm}\frac{\varepsilon_d}{\varepsilon_{250mm}} f_{samplesize} at_{absorbers} at_{sample} COI \tag{3-2}$$

Where

ε_{250mm}	Efficiency curve evaluated at 250 mm from the detector
ε_d	Efficiency at distance d
$f_{samplesize}$	Correction for sample size
$at_{absorbers}$	Correction for gamma-ray attenuation in absorbers
at_{sample}	Correction for gamma-ray attenuation in sample
COI	Coincidence summing correction factor

COI in the detection efficiency refers to the correction factor for true-coincidence summing.

Gamma-rays detected by the detector are usually part of a cascading photons produced in deexcitation processes of an unstable nuclei so they are accompanied by other gamma-rays. By increasing the efficiency of detectors, the simultaneous detection of two photons belonging to the same decay process becomes more probable. If the lifetime of the intermediate levels in the nuclear decay are shorter than the resolving time of the spectrometer, it cannot differentiate between both peaks and the response in the detector would give the same result for the combined peaks of a single pulse. That being said, the total count rate is not affected by the true-coincidence summing [25].

True-coincidence summing has to be taken into account especially when the sample is counted close to the detector.

3.1.2 Interferences

3.1.2.1 Spectral interferences

When analysing a specific energy for each radio nuclide, one can be interfered by gamma-rays emitted by other radio-nuclides. The interfering gamma-rays can be close to each other in terms of energy or even completely overlapped. By using a high resolution germanium detector, some of these interferences can be reduced. In other cases this is corrected by analyzing another peak of the interfering nuclide. By knowing the ratio between the intensity of the peaks we will be able to subtract them from the peak area of the radio-nuclide of interest. For some of these

interferences, corrections are considered in the library for only some of the counting positions. Therefore it is necessary to measure these factors for possible interferences in all counting positions.

This kind of interference is significant especially when both radio-nuclides have similar half-lives or the concentration of the interfering nuclide is high enough to affect the results of the element of interest.

3.1.2.2 Uranium fission interference

Uranium fission interferences are considered as part of nuclear interferences. As explained in the nuclear reactor section, some elements can be produced from fission of ^{235}U such as ^{140}La, ^{141}Ce, ^{153}Sm or ^{147}Nd. If the uranium concentration is in the same range or higher than the concentration of the target radio-nuclide, correction for this interference is necessary. This is dependent on the fission yield, activation cross section and isotopic abundance of the target radio-nuclide. The interference can be calculated roughly from equation (3-3) [52], that is:

$$Int = \frac{4.18 y_i M_x}{238.03 \theta \sigma(n,\gamma)} \tag{3-3}$$

Where

y_i	fission yield of the radio-nuclide
M_x	atomic weight of target element
θ	isotopic abundance of the target element

These factors are included in EPAA's libraries. Measurements were done to determine new correction factors.

3.1.2.3 Neutron self-shielding

During the irradiation, the neutron flux can be perturbed inside the sample. Self-moderation and neutron self-shielding are among the main causes of the neutron flux deviations [25].

Self-moderation: Neutrons can reduce their energy by collision with atoms. By scattering on the light atoms, fast and epithermal neutrons can be thermalized. This phenomenon is more probable in the presence of hydrogen [25].

Neutron self-shielding: A considerable decrease in the neutron flux is observed due to the absorption of neutrons undergoing a neutron capture reaction. If the samples contain high concentrations of elements that strongly absorb thermal neutrons, the inner layers of the sample will see a lower neutron flux. This flux depression is referred to as neutron self-shielding [25, 53, 54]. As an example, mean absorption cross sections for naturally occurring samarium, europium, gadolinium, and dysprosium are 5600, 4300, 49000, and 1100 barns, respectively, indicating that these elements are subject to the neutron self-shielding effect.

This phenomenon can also occur for epithermal neutrons in case of elements with strong resonances of the absorption cross section in the epithermal region.

Case et al.[55] , Dwork [56] and Nisle [57] proposed the first algorithms for neutron self-shielding correction mainly focusing on thermal neutrons. Later on, Stewart and Zweifel derived an expression in which they assume that the neutron flux is isotropic [53, 58]. Algorithms were compiled by Gilat et al. [59], Flemming [60] and integrated in k_0-standardazation by De Corte.

To correct the self-shielding effect in a cylindrical sample with an unknown composition, Chilian et al. [54] introduced a new iterative approach. They proposed equation (3-4) for correcting thermal and epithermal self-shielding.

$$G_{eff} = \frac{f}{f + Q_0(\alpha)} \left[\frac{1.00}{1 + \left(\frac{N_{Av} k_{th}}{r(r+h)} \sum_i \frac{m_i \, \sigma_{abs,i}}{M_{at,i}} \right)^{0.964}} \right] + \frac{Q_0(\alpha)}{f + Q_0(\alpha)} \left[\frac{0.94}{1 + \left(\frac{m \; N_{Av} \, k_{ep} \, \sigma_{abs,ep}}{r(r+h) M_{at}} \right)^{0.82}} + 0.06 \right] \quad (3\text{-}4)$$

Where

m_i	mass of element *i* in the sample
N_A	Avogadro's number
r, h	radius and height of the sample
k_{th}, k_{ep}	thermal and epithermal self-shieling constants
$\sigma_{abs,i}$	thermal neutron absorption cross section for element *i*
$\sigma_{abs,ep}$	epithermal neutron absorption cross section
$M_{at,i}$	atomic mass of element i

3.1.2.4 Gamma ray self-attenuation

Not all the gamma rays that are emitted by the sample reach the detector. A fraction of photons is absorbed or scattered by the material itself and cannot contribute to the peak count-rate. This fraction can cause a considerable error in the analysis especially when dealing with low energy gamma-rays in samples containing heavy elements. This phenomena is referred to as gamma ray self-attenuation and affects the quantification of isotopes such as ^{141}Ce, ^{147}Nd, ^{153}Sm, ^{165}Dy and ^{166}Ho with low energy gamma-rays. Gamma ray self-attenuation effect will increase since the attenuation is a function of energy and the atomic number.

Self-attenuation is dependent on a number of factors such as the sample geometry and the linear attenuation coefficient. The linear attenuation coefficient (μ_x) is a function of the sample's composition, material density and photon energy. For gamma-rays with an intensity of I_0, passing through a length of x in the material, the emerging radiation transmitted by the sample can be expressed as the Beer-Lambert law which is presented in equation (3-5) [61-63]:

$$I = I_0 e^{-\mu_x x} \tag{3-5}$$

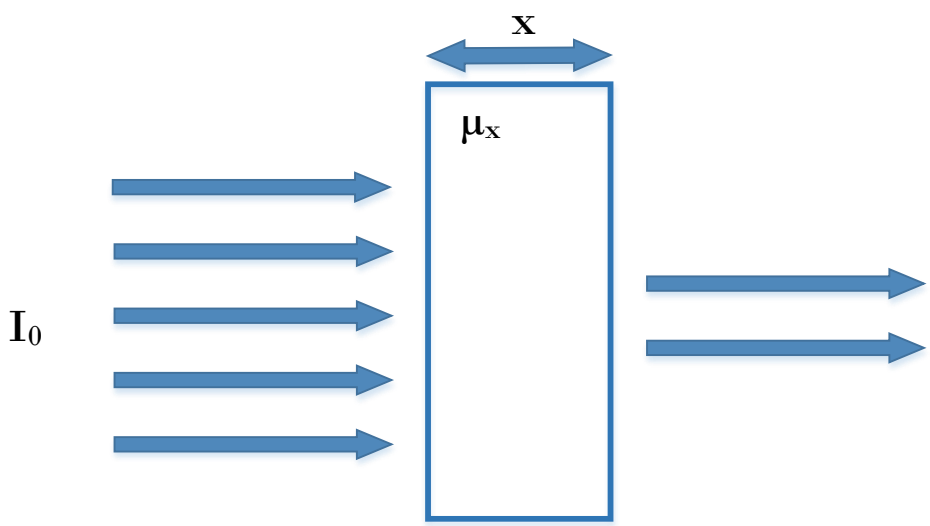

Figure 3-1 Gamma-ray attenuation (adapted from [64])

As illustrated in Figure **3-2**, the attenuation increases when the gamma-ray energy decreases and increases when the absorber gets thicker.

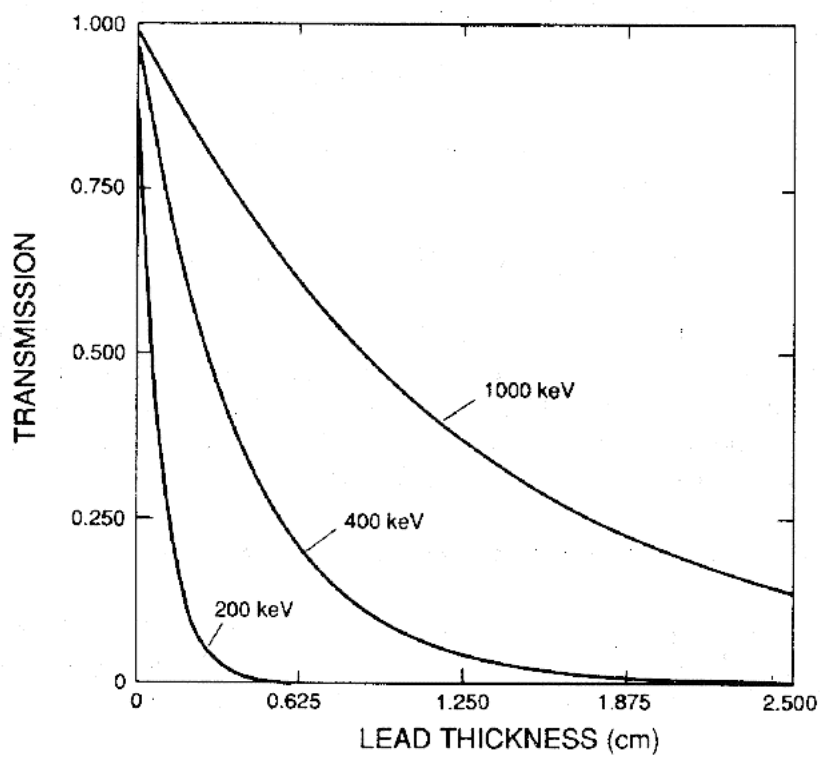

Figure 3-2 Exponential attenuation for three different gamma-ray energies (taken from [64])

As an example, lead which has a high atomic number and density attenuates a much larger fraction of gamma-rays than that of an aluminium medium having the same thickness.

The ratio of the linear attenuation coefficient to the density (μ_x/ρ) is called the mass attenuation coefficient μ with the dimensions of area per unit mass (cm^2g^{-1}). For samples with known compositions the mass attenuation coefficient can be calculated by equation (3-6) [64].

$$\mu = \sum \mu_i w_i \tag{3-6}$$

Where

μ_i mass attenuation coefficient

w_i weight fraction of ith element

However, for a sample with an unknown composition, the value of the linear attenuation coefficient (μ_x) is not known and can be approximated by anticipating the sample composition or estimated by gamma-ray transmission measurements.

The path length a photon travels in the sample is dependent on the sample's geometry and to some extent on the photon energy.

In order to correct for self-attenuation, Sima et al. [65] applied Monte Carlo simulation techniques to calculate the weighted average of the transmission factor by considering the distribution of the path lengths. Dodoo-Amoo et al. suggested working with smaller sample sizes to minimize the self-absorption phenomena [61].

In the EPAA libraries, the attenuation correction is considered in order to correct for this phenomena but the correction is done based on the assumption that the sample has a density of 1.0 g cm^{-3} and that the gamma attenuation coefficient of the sample is made of silica. Therefore, one needs to correct for this effect by taking into account the real density and gamma attenuation coefficients.

Therefore, another objective is to evaluate the self-shielding and gamma-ray attenuation correction modules for samples with high contents of REE.

After investigating all stages of the analysis separately and applying the corrections needed, the final objective would be to evaluate the improved k_0-NAA applied at Polytechnique Montreal.

To achieve the aforementioned objectives, the following steps were followed:

- To investigate the nuclear data and detection efficiency, mono REE standard solutions were tested. These samples are prepared using filter papers to obtain low concentration samples with a similar reproducible geometry. In addition, by analysing each sample for all the rare earth elements, we are able to measure the spectral interferences caused by rare earth elements. Moreover, by analysing uranium and thorium standard solutions we are able to measure the correction factors for the spectral interferences caused by these two elements, as well as the uranium fission interferences.

- To evaluate the neutron self-shielding and gamma ray self-attenuation correction modules, REE oxides were tested. The samples were mixed with SiO_2, in order to produce reproducible geometries.
- After applying the required corrections, a REE certified reference material (CRM) was used to evaluate the performance of the k_0-NAA method for REE determination.

CHAPTER 4 EXPERIMENTAL METHODOLODY

"A theory is something nobody believes, except the person who made it. An experiment is something everybody believes, except the person who made it."

Albert Einstein

This chapter presents the experimental and analytical procedures followed at the SLOWPOKE laboratory in order to determine the concentration of the samples. In addition, a description of the employed facilities, are given.

The experimental procedure for the k_0-NAA analysis includes: Sample preparation, irradiation and counting of the samples followed by the analysis of their spectra, coupled gamma-ray self-attenuation and self-shielding correction and temperature correction.

4.1 Experimental procedures

To verify the libraries applied in EPAA for rare earth elements, samples were prepared from a mono rare earth plasma standard solution, (Specpure® Alfa Aesar) with the concentration of 1000 µg ml^{-1} accurate to 0.3% wt. Approximately 100 µL of the solution was pipetted on the Whatman 42 filter paper with dimensions of 16 mm × 103 mm with polyethylene backing. By using a stopwatch between the beginning of pipetting and weighing, a correction was done in order to take into account the evaporation.

After drying, the filter papers were rolled into 10 mm diameter cylinders, put into 18 mm long polyethylene vials and then heat sealed. The samples were irradiated in the SLOWPOKE reactor with a neutron flux of 5×10^{11} $cm^{-2}s^{-1}$ for 30 min to 90 min and counted on an HPGE detector with 50% efficiency at 1.33 MeV. All samples were counted sequentially at a distance of 1.6 mm (position 1), 33 mm (position 2), or 100 mm (position 3) with respect to the detector. The samples were counted long enough to achieve a net peak area having a statistical error below 0.1 %.

In order to complete the libraries for the spectral and nuclear interference corrections, uranium and thorium samples were prepared in the same manner as the rare earth samples.

Neutron self-shielding and gamma-ray attenuation correction modules were verified by using 100 mg of 99.9% pure rare earth oxides (REO) Alfa Aesar diluted with approximately 1.5g SiO_2. The mono rare earth element oxide samples were irradiated in a neutron flux of 5×10^{11} cm^{-2} s^{-1} for 30 s to 5 min. All the oxides were counted on position 3 to avoid systematic errors introduced by coincidence summing.

A certified reference material (CRM) from Canadian Certified Reference Materials Project, REE-2 [66], was used to validate the k_0-NAA method at the SLOWPOKE laboratory. A 500 mg of REE-2 mixed with 880 mg of SiO_2 was weighed and placed into a 1.4 ml polyethylene vial and irradiated for 2 min. For detecting all the REEs, with different half-lives ranging from hours to years, the sample was counted after 8 hours, 1 day and 8 days decay time.

In addition, Estuarine sediment, BCR-667: IRMM a certified reference material with low REE concentrations was tested. The same irradiation and counting procedure was followed for this CRM.

4.2 Spectra analysis

4.2.1 EPAA

Ecole Polytechnique Activation Analysis (EPAA) software is used as part of the gamma spectroscopy analysis at the SLOWPOKE laboratory. The libraries associated with this software are generated based on the aforementioned k_0 method and detection efficiency model.

The general k_0-formula using a modified Høgdahl convention was presented in section 2.2.4.

After calculating the concentration for the elements of interest, the results were corrected for the gamma ray self-attenuation and the self-shielding effects.

4.2.2 Iterative gamma-ray self-attenuation correction

The gamma-ray attenuation correction within the EPAA software is performed assuming the sample is made of silica and that the density is taken to be 1.0 g cm^{-3}. Since we are dealing with heavy elements which are strong absorbers of gamma-rays we have to take into account the mass attenuation coefficients for each element at the relevant gamma energy. These values are

interpolated from the NIST tables [67]. The degree of attenuation is dependent on factors such as the sample's geometry and the effective mass attenuation coefficient (μ). As previously, explained in section 3.1.2.4, the effective mass attenuation coefficient of the sample at a given gamma-ray can be calculated by equation (3-6).

Therefore, by applying the Beer-Lambert law we are able to calculate the attenuation factor (*f*):

$$f_g = e^{-\mu x \rho} \tag{4-1}$$

Where *x* is the thickness through which the gamma-ray travels. In this work, we assume *x* is equal to one half of the thickness of the sample to simplify the calculations. So by applying an iterative gamma attenuation correction factor to the concentration obtained from EPAA we will be able to correct for this effect by taking into account the real density of the sample.

4.2.3 Iterative neutron self-shielding correction

After correcting the gamma-ray attenuation effect, the iterative neutron self-shielding correction calculations demonstrated by Chilian et al. [54] were applied as presented in section 3.1.2.3.

4.3 SLOWPOKE reactor

The SLOWPOKE reactor at Polytechnique Montréal is a pool type reactor with a thermal power of 20 kW. It was produced and designed by Atomic Energy Canada Limited (AECL) for activation analysis purposes and production of short lived isotopes.

The SLOWPOKE reactor has five inner irradiation sites inside the annular beryllium reflector which are located around the fuel and up to five outer irradiation sites which are located in the surrounding pool water. Irradiation vials are transferred to the reactor and back to the loading station using a pneumatic system. Some design details of the SLOWPOKE reactor are introduced in Table **4-1**.

Table 4-1 SLOWPOKE design specifications

Pool diameter	2.5 m
Pool depth	6.1 m
Container diameter	0.6 m
Container height	5.3 m
Core diameter	22.0 cm
Core height	22.0 cm
Maximum fission power	20.0 kW

The SLOWPOKE reactor is a small research reactor with a reproducible neutron flux in a given irradiation range. The reactor is equipped with a single motor-driven cadmium control rod that moves through a hole in the top reflector to adjust the neutron flux. In this study, the neutron flux was set at 5×10^{11} cm^2 s^{-1} which corresponds to a power of 10 kW. The flux parameters in the inner irradiation sites are $f = 18.0 \pm 0.2$ and $\alpha = -0.051$.

CHAPTER 5 ARTICLE 1: QUANTIFYING REE CONTENT IN HIGH CONCENTRATED SAMPLES BY k_0-NAA

M. Abdollahi Neisiani, M. Latifi, J. Chaouki, C.Chilian

Submitted in Analytica Chimica Acta journal in August 2017

This article presents the main results of the research project.

Abstract The present paper explores the capacity of k_0-NAA for accurate quantification with short turnaround analysis times for rare earth elements (REEs) in high content mineral matrices. REE k_0 and Q_0 values, spectral interferences and nuclear interferences were experimentally evaluated with Alfa Aesar Specpure Plasma Standard 1000 mg kg^{-1} mono-rare earth solutions. The gamma-ray self-attenuation and neutron self-shielding effects were investigated with powder standards prepared from 100 mg of 99.9% Alfa Aesar mono rare earth oxide diluted with silica. The current method was optimized and the overall performance of the improved k_0-NAA method for REEs was validated using a certified reference material (CRM) from Canadian Certified Reference Materials Project (REE-2) with REE content ranging from 7.2 mg kg^{-1} for Yb to 9610 mg kg^{-1} for Ce. The REE concentration was determined with uncertainty below 7% (at 95% confidence level) and proved good consistency with the CRM certified concentrations.

Keywords: k_0-neutron activation analysis, rare earth elements**,** spectral and nuclear interferences, gamma-ray self-attenuation, neutron self-shielding

5.1 Introduction

The rare earth elements are found in the lanthanide series, including scandium and yttrium. Nowadays, REEs have multiple applications in several technologies such as permanent magnets, electronic devices, synthesis of catalysts and those used by the high technology glass industry [1, 2]. REEs go a long way from their natural appearance in fluorocarbonate bastnasite and phosphate monazite to aforementioned end use. The pathway includes exploitation, mining, refining, and waste disposal, and each step requires monitoring REE recovery by quantifying their concentration.

Quantifying REEs is a challenging task due to their similar physical and chemical properties along with generally low amounts and a tendency to come together [3]. Therefore, few instrumental methods, such as ICP-OES, ICP-MS and NAA were able to determine REE with sufficient trueness and precision [4-6]. The drawbacks, limitations and uncertainties associated with each method were analyzed, aiming for a better accuracy of the existing analytical techniques while eliminating error sources.

k_0-Neutron Activation Analysis (k_0-NAA) is a single-comparator, in particular ^{197}Au, standardization method allowing accurate elemental analysis of any material, without the need to recalibrate for all elements when analysing new matrices or using new detectors. Recently k_0-NAA was applied to a limited number of REE determination namely, La, Ce, Nd, Sm, Eu, Tb, Yb, Lu [7, 8], although the method was capable of measuring accurately most of the REE's content at the major, minor and trace levels.

In the last 20 years, k_0-NAA was gradually implemented at Polytechnique Montreal's SLOWPOKE Laboratory [9] but never exploited to its full potential. This was due to the fact that the traditional k_0-NAA method for REEs requires long cooling times for reducing spectral interferences while industrial applications are demanding high accuracy and precision with fast turnaround times.

The k_0-NAA method at Polytechnique Montreal applies the modified Høgdahl convention following equation (5-1):

$$C(\mu g\ g^{-1}) = \frac{peak\ area/t_c}{M\Phi_{th,eq}\ S\ D\ C\ B\ G_{eff}\ C_{mo}\ C_{temp}\ C_{\%full}\ C_{spec\ Interf} C_{nucl\ Interf}} \qquad (5\text{-}1)$$

Where M is the mass of the sample, $\Phi_{th,eq} \sim \Phi_{th}/(1+Q_{0,Au}(\alpha)/f)$ is the thermal neutron flux equivalent to the neutron flux witnessed by the Au monitor, S is the saturation factor $(1-e^{-\lambda t_i})$, D is the decay factor $(1-e^{-\lambda t_d})$ and C is the counting factor $(1-e-^{\lambda t_c})/\lambda t_c$ where t_i, t_d and t_c are irradiation time, decay time and counting time, respectively. G_{eff} is the effective neutron self-shielding factor [10], B is the sensitivity factor, and C_X are correction factors used for the sample neutron moderating effect, neutron temperature effect on reaction rate, % sample filling factor, spectral and nuclear interferences.

Almost all (n, γ) reactions have a *1/v* cross-section behavior, and the sensitivity factor of each radio-isotope, *B*, can be described by the equation (5-2). *B* includes k_0 and Q_0 values for the analyte, the ratio of the thermal and epithermal fluxes *f*, the epithermal neutron flux shape factor α, and the peak relative detection efficiency ε. Moreover, this factor depends on the Avogadro number, N_A, multiplied with the Au isotopic abundance, the Au radiative cross section at 2200 m s^{-1}, the Au 411.8 keV γ-ray intensity and the Au atomic mass.

$$B = \frac{N_{Av}\theta_{Au}\sigma_{0,Au}I_{Au}}{M_{Au}}\ k_0(1 + \frac{Q_0(\alpha)}{f})\varepsilon \qquad (5\text{-}2)$$

Among the *non-1/v* nuclides, ^{152}Eu, ^{152m}Eu, ^{169}Yb and ^{177}Lu have the most extreme deviation and they are analyzed with the k_0-NAA Extended Høghdal convention which introduces new calculated Q_0 values as a function of the neutron temperature and reactor moderator type [11] .These values are used in conjunction with the nuclide specific Westcott $g(T_n)$ factor, where T_n is the neutron temperature [12].

In order to evaluate the k_0-NAA applicability to REE quantification in more than 1000 mg kg^{-1} REE concentrated mineral samples, several sources of systematic error or uncertainty are investigated:

1) Polytechnique Montreal Activation Analysis (EPAA) software
2) Neutron temperature effects
3) Spectral interferences
4) Nuclear interferences for REEs
5) Gamma-ray self-attenuation correction
6) Neutron self-shielding correction

EPAA software libraries are generated based on the k_0-NAA method and the Gunninck detection efficiency model [9]. In these libraries, the k_0 and Q_0 values are embedded together with the detection efficiency in the sensitivity factors, *B*. At Polytechnique Montreal several studies were carried out to verify the accuracy of the method for commonly used nuclides [13] with very little emphasis on REE analysis with k_0-NAA. It was therefore undertaken to assess systematically the effectiveness of the sensitivity constants for all REEs.

Almost all REEs are *non 1/v* thermal neutron absorbers. In most cases, k_0-NAA can be applied with high accuracy because thermal neutron (n,γ) cross section vary almost as 1/v with changing reactor temperature, while the thermal neutron density follows a Maxwell-Boltzmann distribution. The cross sections of the reactions ^{176}Lu(n,γ)^{177}Lu, ^{151}Eu(n, γ)^{152}Eu and ^{168}Yb(n,γ)^{169}Yb have a strong *non*-1/v behaviour and the Westcott formalism for *non-1/v* nuclides is usually applied by adding more complexity to the existing method. Recently the extended Høgdahl convention was proposed for including *1/v* as well as *non-1/v* nuclides in a common method [11], and it was adopted in the present study. For *non-1/v* nuclides the comparison of k_0 and Q_0 values used in the EPAA libraries with the official k_0-NAA database [14] is discussed. The v is the neutron velocity corresponding to a temperature T. Therefore, in the following sections, "neutron temperature" refers to the mean velocity of the thermal neutron density distribution given by the temperature in the irradiation site.

Some of the characteristic γ-rays of REEs are affected by spectral interferences emitted by other radionuclides present in the sample matrix. This interfering radionuclide has several γ-rays other than the interference, and the spectral interference correction factor can be calculated from γ-ray emission probabilities and the corresponding detection efficiency of the interference and another gamma-lines. However, the experimentally determined factors remain more accurate than the calculated ones. In the present study, newly measured and calculated interference correction factors were introduced for improving the analysis with short turnaround times.

The nuclear interferences of REEs yield dominantly from ^{235}U fission which produces light REEs. If not corrected, these interferences could be a source of important errors for uranium samples with concentrations superior to 25 mg kg^{-1}, in particular for elements with radionuclides which are also fission products, as ^{140}La, ^{141}Ce, ^{143}Ce and ^{147}Nd, respectively. In this work, a uranium certified standard solution on filter paper was used to investigate these correction factors, and the experimentally measured uranium fission interference correction factors were compared with the values existing in the literature.

The γ-rays emitted inside the sample could be absorbed or scattered while crossing the sample on their way to the detector, referred to as gamma-ray self-attenuation. This effect introduces analytical errors especially for low energy γ-rays in samples rich in heavy elements. For ^{141}Ce,

^{147}Nd, ^{153}Sm, ^{165}Dy and ^{166}Ho with γ-ray energies under 150 keV, the gamma-ray self-attenuation effect can be as high as 30%, and it was corrected according to the approach of Chilian et al. [15]. During the irradiation, the neutron self-shielding reduces the flux when the sample contain elements with high neutron absorption cross sections, such as Sm, Eu and Gd that are strong absorbers of thermal neutrons, or isotopes such as ^{152}Sm, ^{158}Gd, ^{159}Tb, ^{165}Ho and ^{169}Tm with high resonances in the epithermal region. The thermal and epithermal self-shielding effect are corrected by an improved neutron self-shielding iterative method in accordance with Chilian et al. [10].

5.2 Experimental

In the inner irradiation channels, the thermal neutron flux, Φ_{th}, extends from (5.30 ± 0.3) x 10^{11} $cm^{-2}s^{-1}$ to 5.41 ± 0.3) x 10^{11} $cm^{-2}s^{-1}$ and was re-measured with 10 mm Cu wire monitors with an approximate mass of 25 mg each. Also f =18.1 ± 0.3 is the thermal to epithermal neutron flux ratio and α = -0.051 is epithermal neutron flux shape factor. In fact, f was validated using Cd-ratio measurements with 10 mm long IRMM Al-0.1% Au monitors with an approximate mass of 22 mg each. The monitors were irradiated for 10 minutes and counted 10 cm away from the surface of the detector after a decay time of 24 hours. The net peak area's statistical uncertainty was below 0.1% at 411.8 keV for ^{198}Au and for 511.0 keV for ^{64}Cu.

To verify the accuracy of the sensitivity factors and also to be able to separate all sources of systematic errors, we have prepared calibrators for each REE from certified Alfa Aesar Specpure Plasma Standards which are 1000 mg kg^{-1} solutions accurate to 0.3%. Approximately 100 µL was pipetted on a 16 mm × 103 mm strip of Whatman 42 filter paper with polyethylene backing and weighed immediately. Also, a stopwatch was used to determine and correct the evaporation between the beginning of pipetting and weighing. After drying, the filter paper was rolled into a 10 mm diameter cylinder, put into a 18 mm long polyethylene vial and then heat sealed. Six similar samples were prepared for each solution. The samples were irradiated in the SLOWPOKE reactor at Polytechnique Montreal using a neutron flux of 5×10^{11} cm^{-2} s^{-1} for 30 min to 90 min, and counted on an HPGe detector with a 50% relative efficiency at 1.33 MeV. All samples were counted sequentially at distances of 1.6 mm (P1), 33 mm (P2) and 100 mm (P3) with respect to the detector. The net peak area's statistical error was below 0.1 %.

For completing the libraries with the missing spectral and nuclear interference correction factors, two mono-element pure 100 µg REEs, Th and U calibrators, prepared from an Alfa Aesar Specpure certified standard solution on filter paper were irradiated and counted on each counting position P1, P2 and P3.

Neutron self-shielding and gamma-ray self-attenuation correction models were verified with high concentrated REE samples, using a 100 mg of 99.9% Alfa Aesar rare earth oxides (REO) standard diluted with approximately 1.5 g of SiO_2. Si and O are weak neutron moderators and neutron absorbers. The default EPAA γ-ray detection efficiency model is already designed for a SiO_2 matrix and ^{29}Al, with a half-life of 6.52 min forms by ^{29}Si (n, p)^{29}Al and does not cause any interference for REE analysis. The mono-rare earth element oxide samples were irradiated in a neutron flux of 5×10^{11} cm^{-2} s^{-1} for 30 s to 5 min. All the oxides were counted on position P3 to avoid systematic errors introduced by coincidence summing and geometry effects related to a close-counting set-up [16].

k_0-NAA for REEs was validated with the REE-2 certified reference material from the Canadian Certified Reference Materials Project [17]. That being said, 500 mg of REE-2 mixed with 880 mg SiO_2 was weighed in a 1.4 mL polyethylene vial and irradiated for 2 min. For detecting REE isotopes having different half-lives, the sample was counted after 8 hours, 1 day and 8 days decay time.

For *non 1/v* nuclides, the results were corrected from the default 30ºC to the actual neutron temperature in the irradiation channel by using the $g(T_n)$ values tabulated by van Sluijs et al. [12]. The neutron temperature was estimated based on the reading of the reactor water outlet thermocouple, in this study varying from 29ºC to 50ºC. The errors in concentration introduced by the uncertainty in the temperature determination are estimated as 1% for ^{151}Eu, less than 1% for ^{168}Yb and less than 3% for ^{176}Lu.

5.3 Results and discussion

5.3.1 Sensitivity factors and EPAA libraries

For each chemical element combined with the formed isotope (FI), its half-life and energy of the characteristic γ-ray, EPAA libraries contain three sensitivity factors, *B*, calculated for a sample having a fixed geometry placed in three different reproducible counting positions, P1, P2, and P3. The selection of nuclides, formed isotopes, their γ-rays, k_0 and the Q_0 (with their uncertainty at one standard deviation expressed in %) are presented in Table **5-1**. Most of the data is taken from the official k_0 database [14] with the exception of the Q_0 values for ^{152}Eu, ^{152m}Eu, ^{169}Yb and ^{177}Lu (default neutron temperature of 30°C) from [11] and additionally k_0 and Q_0 for ^{170}Tm from [13].

Table 5-1 Nuclear properties of REE radio isotopes used in this work: gamma energies (γ), k_0 and Q_0 values for target (TI) and formed isotopes (FI)

TI	FI	$T_{1/2}$	γ (keV)	k_0	(%; 1s)	Q_0	(%; 1s)
^{139}La	^{140}La	1.678 d	1596.2	1.34E-01	(1.1)	1.24	(5.0)
^{140}Ce	^{141}Ce	32.51 d	145.4	3.66E-03	(0.9)	0.83	(5.0)
^{142}Ce	^{143}Ce	33.1 h	293.3	6.89E-04	(0.5)	1.2	(5.0)
^{141}Pr	^{142}Pr	19.12 h	1575.6	6.12E-03	(0.6)	1.51	(5.0)
^{146}Nd	^{147}Nd	10.98 d	91.1	1.02E-03	(2.5)	2	(1.2)
^{146}Nd	^{147}Nd	10.98 d	531	4.56E-04	(1.1)	2	(1.2)
^{152}Sm	^{153}Sm	46.5 h	103.2	2.31E-01	(0.4)	14.4	(2.1)
^{151}Eu	^{152}Eu	13.54 y	1408	9.36E+00	(0.6)	0.66[a]	(5.0)
^{151}Eu	^{152m}Eu	9.312 h	841.6	3.02E+00	(5.0)	0.66[a]	(5.0)
^{151}Eu	^{152m}Eu	9.312 h	963.3	2.49E+00	(5.0)	0.66[a]	(5.0)
^{152}Gd	^{153}Gd	240.4 d	103.2	4.54E-03	(4.0)	0.77	(15.0)
^{158}Gd	^{159}Gd	18.56 h	363.5	8.49E-04	(1.6)	29.9	(3.1)
^{159}Tb	^{160}Tb	72.3 d	298.6	8.25E-02	(1.2)	17.9	(3.8)
^{159}Tb	^{160}Tb	72.3 d	879.4	9.42E-02	(0.9)	17.9	(3.8)
^{164}Dy	^{165}Dy	2.334 h	94.7	3.57E-01	(1.4)	0.19	(5.0)
^{165}Ho	^{166}Ho	26.83 h	80.6	4.94E-02	(1.0)	10.9	(2.4)
^{170}Er	^{171}Er	7.516 h	308.3	1.04E-02	(1.4)	4.42	(3.3)
^{169}Tm	^{170}Tm	128.6 d	84.3	3.45E-02[b]	(2.5)	14.3[b]	(2.1)
^{168}Yb	^{169}Yb	32.03 d	177.2	1.04E-02	(5.0)	10.8[a]	(5.0)
^{168}Yb	^{169}Yb	32.03 d	198	1.64E-02	(5.0)	4.97[a]	(5.0)
^{174}Yb	^{175}Yb	4.185 d	396.3	3.12E-02	(0.6)	0.46	(5.0)
^{176}Lu	^{177}Lu	6.73 d	208.4	7.14E-02	(5.0)	3.49[a]	(5.0)

[a] Q_0 values for a temperature of 30 ºC, Van Sluijs [11]

[b] k_0 and Q_0 values for ^{169}Tm, St-Pierre et al. [13]

The EPAA libraries consider a gamma-ray self-attenuation correction for a sample of 1.00 kg m^{-3} density, which is different from the real filter sample density of 0.15 kg m^{-3}. Therefore, the new detection efficiencies were calculated in order to take into account for this difference. The neutron self-shielding correction is less than 0.2 % for almost all REEs and it was not corrected, with the exception of Gd, where a 1.5% correction was applied.

The correction for true-coincidence summing is essential when k_0-NAA is employed with low flux reactors leading to close-counting geometries. Since the efficiency model is dependent on the sample-detector geometry, by analyzing the data obtained in position P1, we can elaborate on the detection efficiency calibration and its true coincidence summing correction (COI). As the distance between the sample and the detector is increasing, the COI is decreasing below 2%. Therefore, data obtained by counting the sample on position P3 can be used to investigate the $k_0(1+ Q_0(\alpha)/f)$ values for *1/v* nuclides and $k_0(g(T_n)+Q_0(\alpha)/f)$ values for *non 1/v* nuclides, respectively.

The results for each REE were normalized to the weighted content, and the range of the individual REE dataset was approximately 10%. In this manner, the measured value is the average, with an uncertainty of 2% at one standard deviation (*1s*), with the exception of Lu and Eu, where the uncertainty is 4% and respectively 3%, respectively. The mean values are presented in Table **5-2** along with the COI factors for all three counting positions P1, P2, and P3.

Table 5-2 Concentrations for the REE solutions on filter paper (X_p), normalized with respect to the standard certified values (X_{cert}) and corresponding coincidence summing correction factors (COI) for three different counting positions P1, P2 and P3

FI	γ (keV)	X_{P1}/X_{cert}	COI_{P1}	X_{P2}/X_{cert}	COI_{P2}	X_{P3}/X_{cert}	COI_{P3}
^{140}La	1596.2	0.95	0.80	0.94	0.93	0.97	0.98
^{141}Ce	145.4	1.00	1.00	0.96	1.00	0.99	1.00
^{143}Ce	293.3	1.03	0.94	0.98	0.98	0.96	0.99
^{142}Pr	1576.6	0.99	1.00	1.00	1.00	1.00	1.00
^{147}Nd	91.1	0.97	0.99	0.96	1.00	0.99	1.00
^{147}Nd	531.0	1.00	1.00	0.96	1.00	1.01	1.00
^{153}Sm	103.2	0.99	0.98	0.95	0.99	0.97	1.00
^{152}Eu	1408	1.03	0.88	0.96	0.95	0.99	0.99
^{152m}Eu	841.6	1.15	0.87	1.09	0.95	1.09	0.99
^{152m}Eu	963.3	1.13	1.05	1.06	1.01	1.08	1.00
^{153}Gd	103.2	1.04	0.96	1.02	0.98	1.03	1.00
^{159}Gd	363.5	1.01	1.00	0.98	1.00	1.01	1.00
^{160}Tb	298.6	0.96	0.83	0.95	0.94	0.97	0.98
^{160}Tb	879.4	1.03	0.87	0.99	0.95	1.00	0.99
^{165}Dy	94.7	1.00	1.00	0.96	1.00	0.98	1.00
^{166}Ho	80.6	0.99	1.00	0.97	1.00	0.99	1.00
^{171}Er	308.3	0.98	0.89	0.95	0.96	0.97	0.99
^{170}Tm	84.3	1.00	1.00	0.97	1.00	0.99	1.00
^{169}Yb	177.2	1.04	0.72	0.91	0.89	0.87	0.97
^{169}Yb	198.0	0.99	0.77	0.91	0.90	0.86	0.98
^{175}Yb	396.3	1.00	1.02	0.98	1.01	0.99	1.00
^{177}Lu	208.4	0.97	0.90	0.95	0.96	0.97	0.99

In the case of free true coincidence summing correction isotopes: ^{142}Pr, ^{147}Nd (531 keV), ^{159}Gd, and ^{175}Yb, of relatively high energy γ-lines, and ^{141}Ce, ^{147}Nd (91.1 keV), ^{153}Sm, ^{165}Dy, ^{166}Ho, ^{170}Tm, with energies below 150 keV, the analytical results for position P1 and P3, present absolute biases within the 2-3% of the experimental uncertainty at *1s*. These results validate the detection efficiency model and also the k_0 and Q_0 values. Therefore, the sensitivity factors of these REEs are sufficiently accurate for high and low energy γ-lines and additionally for samples counted in a close or far detection geometry. On the contrary, for the same isotopes, the results obtained for position P2 are reporting consistent negative biases of 2% to 5%, provided from the underestimation of 1 mm of the sample/detector distance used for calculating the detection efficiencies for position P2. This error was corrected and all further experimental results were calculated with the corrected library for P2.

Moreover, ^{140}La, ^{143}Ce, ^{152m}Eu (841.6 keV), ^{152}Eu, ^{153}Gd, ^{160}Tb, ^{171}Er, ^{169}Yb and ^{177}Lu peaks are subject to summing-out true coincidence effects, while ^{175}Yb (396 keV) and ^{152m}Eu (963.3 keV) peaks are affected by summing-in true coincidence summing effect. The 3% negative biases for ^{140}La and ^{171}Er are witnessed in all experimental results and could be generated by the COI inaccuracy; this was accounted for by considering them as systematic errors in the following analyses.

If the negative bias in position P3 for ^{143}Ce is eliminated by reducing the sensitivity factor accordingly, the bias in position P1 increases and points to the COI as the source of the error. However, no action was taken to correct the library and these errors were added to the uncertainty budget.

Apparently, COI over-corrects for ^{152}Eu (1408 keV) and ^{60}Tb (879 keV) counted in position P1, since the biases in position P3 are below 1%. For ^{160}Tb (299 keV) the negative biases of 4% in P1 and 3% in P3 are inconclusive, and it could be associated equally to COI or to inconsistencies in the k_0 and Q_0 values. This uncertainty is added to the uncertainty budget of further results obtained through the ^{160}Tb (299 keV) γ-line.

In position P1, ^{152m}Eu results for 842 keV and 963 keV present large positive biases of 13% and 15% that decrease to 9% and 8%, respectively, for the results in position P3. With the assumption that Q_0 and $g(T_n)$ values [11] are acceptable, the ^{152}Eu (1408 keV) results confirm that its k_0 value

is sufficiently accurate, while for ^{152m}Eu (841 keV) the k_0 factor is situated around 3.26 and for ^{152m}Eu (963 keV) around 2.68, values that are 8% higher than the one reported in the official database. If the sensitivity factors for these two cases are increased by 8%, the bias of the results in position P1 decreases to approximately 6% indicating a systematic error in the COI correction. Therewith, the ^{177}Lu (204 keV) experimental result in positions P1 and P3 has a bias within the 4% limit of measured uncertainty, validating the sensitivity factors and implicitly the detection efficiency model and k_0 and Q_0 values of ^{177}Lu (204 keV). When counting on P3, both ^{169}Yb gamma lines, 177 keV and 198 keV, give results of 13-14% negative bias. Once again, if Q_0 and $g(T_n)$ values remain constant in the library, both k_0 values seems to be 13-14% lower than the values reported in the official k_0-database. This assumption implies a dramatic increase for the positive biases witnessed for the results obtained in position P1. Until a thorough investigation is done to elucidate the ^{169}Yb case, we choose ^{175}Yb (396 keV) for any future ytterbium analysis.

In addition, ^{153}Gd (103 keV) results have a consistent positive bias of 3% in P1 and P3 and it can be generated by the presence, at the trace level, of the samarium very sensitive to neutron activation, forming ^{153}Sm (103 keV). The decay protocol of maximum 8 days is unfavorable for the ^{153}Gd half-life of 240 days, comparatively with ^{153}Sm half-life of 46 hours and therefore the option of analysing gadolinium with this formed isotope was abandoned.

It should be mentioned that Polytechnique's detection efficiency model has the roots in the approach [18]. The equations presented in this reference were implemented in the real detection efficiency calculation with additional undocumented corrections, the COI correction was apparently changed, the new approach is not revealed and it was reported as introducing systematic errors when investigated for some special cases [16].

Finally, it should be acknowledged that the EPAA software does not take into account the cases when the k_0 values are calculated differently. As an example the nuclides associated with a decay type IV/b corresponding to "two-component decay", which pass through a metastable state with a significantly lower half-life than that of the ground state used in the analysis. EPAA considers all reactions as type I or "beta-beta", except for a few cases such as ^{80}Br, ^{99}Mo and ^{115}Cd where a fixed correction factor is applied for a default decay time. For example, (^{165m}Dy 1.26 min, ^{165}Dy 2.33 hours, 94.7 keV) type II or "isomeric transition-beta" decay is not respected. There are other

two-component decay relevant cases to REE that have not been considered in EPAA, namely, (^{233}Th 22.2 min, ^{233}Pa 27.0 d, 312 keV) and (^{239}U 23.5 min, ^{239}Np 2.35 days). To overcome this weakness, the sample cooling time was chosen to be sufficiently long in order to avoid introducing the errors associated with the competing decay of the metastable state; this was achieved with a decay protocol of 8 hours, 1 day and 8 days, respectively.

5.3.1.1 C_{mo} and $C_{\%}$ correction factors

In the present work, C_{mo} and $C_{\%}$ in equation (5-1) can be disregarded. In fact, C_{mo}= 1 because the samples do not contain moderator materials such as hydrogen and in addition the epithermal and fast neutrons are not thermalized by colliding with the moderating atoms which leads to a change in the neutron flux. Moreover, $C_{\%}$ = 1 since all samples were prepared with a 100% filling factor of the vial. In this way the counting geometry is reproducible and the systematic errors introduced by the detection efficiency model for lower filling factors are avoided [16].

5.3.1.2 C_{temp} correction factor

The C_{temp} correction refers to the changes in the activation rate due to the variation of the neutron radiative capture cross section with neutron temperature, and should not be confused with the case of *non 1/v* nuclides. The SLOWPOKE reactor neutron flux detector is Cd self-powered with a *non 1/v* conversion factor of the thermal neutron flux to the detector's electric signal. With the increase of the reactor temperature, as the ^{235}U fission rate with thermal neutrons and Be reflector moderating properties are reduced, the reactor control rod withdraws for maintaining a constant electrical current from Cd neutron detector, equivalent to a constant thermal activation rate. Both actions, including an increase of the temperature and withdrawal of the control rod, produce a change in the shape of neutron spectrum and also to the ratio of thermal to epithermal neutron flux, f. For the $1/$v nuclides, the C_{temp} correction was done according to the reading of the reactor water outlet and inlet thermocouples and it ranges from 0.5% to maximum 3%. Since f (and accordingly α) will decrease with the increase of the temperature, this correction introduces small systematic errors, expected to be lower than 2% for nuclides with Q_0 values higher than 30.

5.3.1.3 $C_{spec\ interf}$ spectral interference correction factor

In addition to sensitivity factors, EPAA's previous libraries included few corrections for spectral and nuclear interferences, $C_{spec\ interf}$, as indicated in Table **5-3** Spectral Interference Correction Factors for three different counting positions, (P1, P2, P3) for the data marked with the superscript "a". As an example: ^{141}Ce 145 keV γ-line is interfered by ^{175}Yb 144 keV γ-line, but a correction factor is provided just for the counting position P1. Uranium is measured by the decay of ^{239}Np with a γ-ray at 104 keV interfering with 103 keV γ-line of ^{153}Sm and once again the correction factor is given just for the position P2. For a consistent approach, correction factors were necessary for all counting position, especially when high content REE samples impose counting far from the detector, at position P3. For accurate correction factors, their experimental determination is suitable since it eliminates the errors introduced by the detection efficiency model, including the counting geometry model and the true-coincidence summing. When the experimental approach is difficult, as in the case of the 842 keV and 963 keV γ-lines of ^{152m}Eu interfered by 842 keV and 963 keV γ-lines of ^{152}Eu, the correction factors were calculated from the γ-ray intensities and their corresponding detection efficiency.

The isotope ^{133}I is a ^{235}U fission product which could interfere with the ^{147}Nd 531 keV peak in uranium bearing matrices, but can be neglected for high neodymium content samples depleted in uranium or it can be avoided by increasing the decay time. Also, ^{153}Sm interferes with ^{147}Nd 531 keV and even when the correction factor is very small the interference is taken in consideration for potential depleted neodymium samples. Another ^{235}U fission product, ^{131}I which represents a potential significant spectral interference for ^{159}Gd 363 keV peak. In addition, ^{233}Pa (27 days) has a γ-line at 104 keV which can potentially interfere with the 103 keV γ-line of ^{153}Sm (1.9 days) but the magnitude of the interference is relatively low due to the half-life difference between the two isotopes and a sensitivity ten times higher for the ^{152}Sm than the ^{232}Th. Another few similar cases are the interferences of ^{233}Pa on the 94.7 keV of ^{165}Dy, ^{239}Np on the 80.6 keV of ^{166}Ho, ^{169}Yb on the 308 keV of ^{171}Er and ^{160}Tb on the 198 keV of ^{169}Yb. Correction factors were measured (or calculated when the statistical uncertainty of the surface of the interfering peak was higher than 20%) for each counting position and added to the library. The all new spectral interference correction factors which were experimentally measured or calculated (in italic) are included in Table **5-3**.

Table 5-3 Spectral Interference Correction Factors for three different counting positions, (P1, P2, P3)

FI	γ (keV)	$T_{1/2}$	SII	$\gamma_{SIIinterf}$ (keV)	γ_{SII} (keV)	$T_{1/2}$	P1	P2	P3
^{141}Ce	145.4	32.5 d	^{175}Yb	144.9	396.3	4.19 d	0.073[a]	0.088	0.090
^{147}Nd	531.0	11.0 d	^{153}Sm	531.4	103.2	46.5 h	0.001	0.001	0.001
			^{133}I (U fiss)	529.8	875.3	20.8 h	*45.6*	*32.4*	*28.5*
^{153}Sm	103.2	46.5 h	^{233}Pa	103.9	312.0	27.0 d	0.023	0.027	0.028
			^{239}Np (U)	103.7	277.6	2.35 d	1.817	1.901[a]	1.777
^{152m}Eu	841.6	9.31 h	^{152}Eu	841.6	1408.0	13.5 y	*0.011*	*0.011*	*0.011*
^{152m}Eu	963.3	9.31 h	^{152}Eu	964.1	1408.0	13.5 y	*1.135*	*0.971*	*0.912*
^{159}Gd	363.5	18.6 h	^{131}I (U fiss)	364.5	637.0	8.04 d	*17.0*	*16.8*	*16.4*
^{160}Tb	298.6	72.3 d	^{233}Pa (Th)	300.2	312.0	27.0 d	0.178[a]	0.169[a]	0.171
^{165}Dy	94.7	2.33 h	^{233}Pa	94.7	312.0	27.0 d	0.281	0.280	0.275
^{166}Ho	80.6	26.8 h	^{239}Np	Experimental	277.6	2.36 d	0.001	0.008	0.008
^{171}Er	308.3	7.52 h	^{169}Yb	307.7	198.0	32.0 d	*0.275*	*0.244*	*0.238*
^{169}Yb	198.0	32.0 d	^{160}Tb	197.0	879.0	72.3 d	*0.471*	*0.507*	*0.494*
^{175}Yb	396.3	4.19 d	^{140}La	397.7	1596.0	1.68 d	*0.022*	*0.020[a]*	*0.021*
			^{147}Nd	398.2	91.1	11.0 d	*0.028*	*0.027[a]*	*0.028*
			^{233}Pa (Th)	398.7	312.0	27.0 d	0.032[a]	0.030[a]	0.031
^{177}Lu	208.4	6.73 d	^{239}Np (U)	209.8	277.6	2.36 d	0.352[a]	0.301[a]	0.283

[a] Existing spectral correction interference factors in the old EPAA libraries

[b] The spectral interference correction factor related to ^{233}Pa(Th) comprises two contributions: 298.9 keV (0.03%) and 300.2 keV (6.20%)

5.3.1.4 $C_{nucl\ interf}$ nuclear interference correction factor

The nuclear interferences from the second-order reactions, ^{151}Eu on ^{153}Gd and ^{164}Dy on ^{166}Ho, are insignificant since the samples are highly concentrated in REEs and also because they are irradiated for just a few minutes in a low neutron flux reactor [19].

For samples containing uranium, elements such as La, Ce and Nd can be affected by fission interferences if the uranium content exceeds those of the light REEs [20]. In this case, ^{140}La, ^{141}Ce and ^{147}Nd, isotopes that are selected for measuring the concentration of the related elements, are also produced from the uranium fission process. The correction factors, $C_{nucl\ interf}$ were calculated by measuring the amount of each isotope produced per unit mass of standard uranium.

Table **5-4** presents the REEs affected by uranium fission interferences. The theoretical values calculated from REE fission yield values recently proposed by Tiwari et al. [7] and the uranium fission interference correction factors measured in this work.

Table 5-4 Uranium Fission Interference Correction Factors for REEs

Element	FI	γ (keV)	Theoretical	Ref.7	EPAA	This work
La	^{140}La	1596.2	0.016	0.0027	0.00238	0.00231
Ce	^{141}Ce	145.4	0.28	0.34	0.28	0.282
	^{143}Ce	293.3	1.33	1.35	1.25	1.28
Nd	^{147}Nd	91.1	0.22	0.20	0.23	0.190

5.3.2 Gamma-ray self-attenuation and Neutron self-shielding

The REE oxides were used to investigate the correction models for gamma-ray self-attenuation and neutron self-shielding in extreme cases, as presented in Table **5-5**. In order to avoid systematic errors introduced by the detection efficiency model for a close-counting geometry, the samples were counted 100 mm away from the detector, at position P3.

EPAA libraries assume a SiO_2 matrix of density equal to 1.0 kg m^{-3}. If gamma-ray self-attenuation is not calculated for the actual sample density and composition, it can introduce biases as high as 30% for elements analysed with nuclides emitting low energy γ-rays which are easily absorbed in a matrixes containing heavy elements [15]. In the present study, an iterative method was implemented in order to correct for gamma-ray self-attenuation for unknown composition samples. To simplify the calculation, we assumed the average path of γ-ray in the sample equal to one half of the averaged thickness of the sample. The attenuation coefficient is a function of material density, sample composition, and γ-ray energy. Using elemental mass attenuation coefficients interpolated from the NIST tables [21] and by applying the Beer-Lambert law we were able to calculate the matrix mass attenuation coefficient for each γ-ray energy. The performance of the gamma-ray self-attenuation method for high concentrated mono-REE is presented in the Table **5-5**.

Table 5-5 Comparison of REE concentrations in oxides measured at different steps of k_0-NAA with respect to the certified values (X_{cert}): concentration obtained from EPAA (X_{EPAA}), after self-shielding correction ($X_{ss\ corr}$), after γ-ray attenuation correction ($X_{GA\ corr}$)

FI	γ (keV)	X_{cert}(%wt)	X_{EPAA}/ X_{cert}	$X_{SS\ corr}$/ X_{cert}	$X_{GA\ corr}$/ X_{cert}
^{140}La	1596.2	0.86	0.93	0.95	0.95
^{141}Ce	145.4	0.81	0.93	0.93	1.03
^{143}Ce	293.3	0.81	0.97	0.97	0.98
^{147}Nd	91.1	0.86	0.82	0.84	1.02
^{147}Nd	531.0	0.86	0.99	1.01	1.01
^{153}Sm	103.2	0.86	0.25	0.67	0.92
^{152}Eu	1408	0.86	0.41	0.93	0.93
^{152m}Eu	841.6	0.86	0.42	1.01	1.01
^{152m}Eu	963.3	0.86	0.43	1.05	1.05
^{159}Gd	363.5	0.87	0.65	1.02	1.02
^{160}Tb	298.6	0.85	0.79	0.98	0.98
^{160}Tb	879.4	0.85	0.82	1.01	1.01
^{165}Dy	94.7	0.87	0.74	0.86	1.03
^{166}Ho	80.6	0.87	0.73	0.82	1.04
^{171}Er	308.3	0.87	0.87	0.94	0.94
^{170}Tm	84.3	0.87	0.54	0.69	0.94
^{169}Yb	177.2	0.88	0.91	0.93	0.98
^{169}Yb	198.0	0.88	0.94	0.95	1.01
^{175}Yb	396.3	0.88	0.94	0.95	0.95
^{177}Lu	208.4	0.88	0.89	0.91	0.96

Thermal and epithermal self-shielding effects introduce errors in the analysis of strong absorbers of thermal neutrons such as samarium, europium and gadolinium, or for ^{152}Sm, ^{158}Gd, ^{159}Tb, ^{165}Ho and ^{169}Tm having high resonance absorption cross sections. Polytechnique Montreal Neutron Self-Shielding (POLY-NSS), is an iterative method correcting the neutron self-shielding for cylindrical samples of unknown composition following the method of Chilian et al. [10]. POLY-NSS was updated with new G_{eff} factors calculated from the ENDF/B-VII.1 nuclear database, with the exception of platinum isotopes for which the resonance parameters were taken from TENDL-2012 nuclear database. The epithermal neutron self-shielding for *non 1/v* nuclides, ^{152}Eu, ^{152m}Eu, ^{169}Yb, and ^{177}Lu, was calculated with the Q_0 (and the, energy of resonance, E_r) of the Extended Høghdal convention [11].

The results presented in Table 5 are normalized to the certified concentration of the mono-REE oxides. When correcting for gamma-ray self-attenuation in the case of ^{147}Nd (91.1 keV), ^{165}Dy (94.7 keV), ^{166}Ho (80.6 keV) and ^{170}Tm (84.3 keV), a 10% to 22% γ-ray attenuation correction introduces a maximum positive bias of 5%, which reduces as the correction becomes less significant. The positive bias is explained by the underestimation of the average path of γ-ray in the sample introduced by the model [15]. As expected, POLY-NSS demonstrated sufficient accuracy when correcting 40% or 30% neutron self-shielding for the extreme cases of europium and samarium respectively. Moreover, the iterative calculation is accurate even for correcting a 67% combined effect, as it was in the case for samarium.

We can conclude that the uncertainty associated with the correction of these two effects is 5% for coupled effects that are less than 20%, and increases to 9% when correcting for more than 20% combined gamma-ray self-attenuation and neutron self-shielding effects.

5.3.3 Validation of k_0-NAA for REEs

The performance of the k_0-NAA for quantification of REEs was investigated with a REE-2 certified reference material from Canadian Certified Reference Materials Project, and the results are reported in Table **5-6**.

Table 5-6 Comparison of measured REE concentrations (X_{lab}) with the certified values (X_{cert}) at different steps of k_0-NAA: concentration obtained from EPAA (X_{EPAA}), after self-shielding correction ($X_{ss\ corr}$), after γ-ray attenuation correction ($X_{GA\ corr}$)

El	FI	γ (keV)	$X_{cert} \pm u_{cert}$ (mg kg^{-1})		X_{EPAA}/X_{cert}	$X_{SS\ corr}/X_{cer}$	$X_{GA\ corr}/X_{cert}$	$X_{lab} \pm u_{lab}$(mg kg^{-1})	
La	^{140}La	1596.2	5130	± 50	0.97	0.99	0.99	5058	± 168
Ce	^{141}Ce	145.4	9610	± 160	0.93	0.95	0.98	9428	± 404
Ce	^{143}Ce	293.3	9610	± 160	0.95	0.97	0.97	9303	± 483
Pr	^{142}Pr	1576.6	1075	± 26	0.97	0.99	0.99	1067	± 36
Nd	^{147}Nd	91.1	3660	± 70	0.89	0.91	0.95	3491	± 183
Nd	^{147}Nd	531.0	3660	± 70	0.99	1.01	1.01	3702	± 129
Sm	^{153}Sm	103.2	410	± 7	0.94	0.96	1.00	409	± 17
Eu	^{152}Eu	1408.0	96.6	± 2.5	1.00	1.02	1.02	98.8	± 5.9
Eu	^{152m}Eu	841.6	96.6	± 2.5	1.00	1.02	1.02	98.6	± 5.59
Eu	^{152m}Eu	963.3	96.6	± 2.5	0.99	1.01	1.01	98.0	± 3.19
Gd	^{159}Gd	363.5	219	± 10	0.91	0.92	0.92	201	± 16.1
Tb	^{160}Tb	298.6	20.3	± 0.7	0.89	0.90	0.90	18.3	± 1.82
Tb	^{160}Tb	879.4	20.3	± 0.7	0.97	0.99	0.99	20.0	± 1.66
Dy	^{165}Dy	94.7	69.2	± 0.8	0.93	0.95	0.99	68.8	± 3.37
Ho	^{166}Ho	80.6	7.87	± 0.25	1.00	1.01	1.07	8.41	± 0.78
Er	^{171}Er	308.3	14.0	± 2.1	-	-	-	<22	-
Tm	^{170}Tm	84.3	1.383	± 0.022	-	-	-	<13	-
Yb	^{175}Yb	396.3	7.2	± 0.5	-	-	-	<11	-
Lu	^{177}Lu	208.4	0.92	± 0.07	1.45	1.48	1.51	1.39	± 0.16
Th	^{233}Pa	312.0	737	± 14	0.97	0.98	0.98	724	± 25.6
U	^{239}Np	277.60	3.73	±0.12	-	-	-	<4.9	-

The overall combined standard uncertainty was calculated in quadrature of the squares of the all uncertainty components mentioned in Table **5-7**.

Table 5-7 Uncertainty components for the determination of REE-2 by k_0-NAA

Source	**Typical range**
Mass of sample	0.1%
Counting statistics	0.1% - 20%
$k_0(g(T_n) + Q_0(\alpha)/f)$	3% -7%
Detection efficiency - geometry effects	1% - 3%
Detection efficiency - gamma-ray self-attenuation	0% - 5%
Irradiation, counting, decay time	negligible
Gamma-ray interferences	0.2%
Fission interferences	0%
Neutron temperature effects	0.1% - 3%
Neutron self-shielding	0% - 3%

Agreement of the element content found by k_0-NAA with the REE-2 certified values was tested with the E_n number defined by ISO Guide 13528 [22]. Discrepancies in the results were found for terbium that was measured with ^{160}Tb (297 keV) with E_n = 1.08 and lutetium with E_n = 2.76. The result obtained with ^{160}Tb (297 keV) correspond to position P1 and the true coincidence correction could be responsible for the small discrepancy of 1.08. However, for Lu, the large discrepancy has no apparent explanation, and the discrepancy persisted when a second REE-2 sample was analysed.

Therefore, k_0-NAA failed to quantify thulium and ytterbium in REE-2 due to their low concentration at mg kg^{-1} level, low energy gamma-lines, and 8 days short decay time.

5.4 Conclusions

The present study critically assessed the performance of the k_0-NAA mehtod for quantifying REEs in highly concentrated samples. The EPAA sensitivity factors were experimentally validated or corrected when necessary. EPAA libraries were completed with new spectral and nuclear interference corrections factors. It was found that the k_0 and Q_0 data for ^{169}Yb (177 and 198 keV) and ^{177}Lu (208 keV) need to be further analyzed. Inconsistencies in correcting the true coincidence summing effects indicated that COI factors are not accurate; therefore, the method is under investigation. The gamma-ray self-attenuation coupled with the neutron self-shielding iterative calculation is sufficiently accurate even for correcting 67% combined effect, as it was the case for samarium.

It was proven that 10 REEs can be accurately measured by k_0-NAA at Polytechnique Montreal SLOWPOKE Laboratory with turnaround times of 8 days. The maturity of the method leads us to believe that k_0-NAA can be extended up to 12 REEs.

5.5 Acknowledgements

The authors would like to acknowledge Natural Sciences and Engineering Research Council of Canada (NSERC) and Niobec, a Magris Resources Company for funding this research through the Collaborative Research and Development Program.

5.6 References

1. Commission, E., *Report on Critical Raw materials for the EU.* Retrieved April, 2014. **30**: p. 2015.
2. Energy, U.S.D.o., *Critical materials strategy*. 2010: US Department of Energy.
3. McDonough, W.F. and S.-S. Sun, *The composition of the Earth.* Chemical geology, 1995. **120**(3-4): p. 223-253.
4. Bulska, E., et al., *Inductively coupled plasma mass spectrometry in comparison with neutron activation and ion chromatography with UV/VIS detection for the determination of lanthanides in plant materials.* Talanta, 2012. **97**: p. 303-311.
5. D'Angelo, J.A., et al., *Determination of eight lanthanides in apatites by ICP-AES, XRF, and NAA.* Journal of trace and microprobe techniques, 2001. **19**(1): p. 79-90.
6. Dybczyński, R.S., et al., *Comparison of performance of INAA, RNAA and ion chromatography for the determination of individual lanthanides.* Applied Radiation and Isotopes, 2010. **68**(1): p. 23-27.

7. Tiwari, S., et al., *Analysis of uranium bearing samples for rare earth and other elements by k0-based internal monostandard INAA method.* Journal of Nuclear and Radiochemical Sciences, 2007. **8**(1): p. 25-30.
8. Xiao, C., et al., *k0-NAA for determination of REE in reference materials of ore sources.* Journal of Radioanalytical and Nuclear Chemistry, 2017. **311**(2): p. 1287-1289.
9. Chilian, C. and G. Kennedy, *The NAA method at Polytechnique Montreal: an efficient alternative way to use the k0 NAA models.* Journal of Radioanalytical and Nuclear Chemistry, 2014. **300**(2): p. 533-538.
10. Chilian, C., J. St-Pierre, and G. Kennedy, *Complete thermal and epithermal neutron self-shielding corrections for NAA using a spreadsheet.* Journal of radioanalytical and nuclear chemistry, 2008. **278**(3): p. 745-749.
11. van Sluijs, R., *Q 0's and resonance energies used in k 0-NAA compared with estimations based on ENDF/B-VII. 1 cross section data.* Journal of Radioanalytical and Nuclear Chemistry, 2016. **309**(1): p. 219-228.
12. van Sluijs, R., A. Stopic, and R. Jacimovic, *Evaluation of Westcott g (Tn)-factors used in k0-NAA for "non-1/v"(n, γ) reactions.* Journal of Radioanalytical and Nuclear Chemistry, 2015. **306**(3): p. 579-587.
13. St-Pierre, J. and G. Kennedy, *Re-measurement of Q 0 and k 0 values for 14 nuclides.* Nuclear Instruments and Methods in Physics Research Section A: Accelerators, Spectrometers, Detectors and Associated Equipment, 2006. **564**(2): p. 669-674.
14. Jaćimović, R., et al., *The 2012 recommended k0 database.* Journal of Radioanalytical and Nuclear Chemistry, 2014. **300**(2): p. 589-592.
15. Chilian, C. and C. Lacroix, *Towards routine NAA of materials rich in heavy elements with iterative gamma-ray attenuation and neutron self-shielding calculations.* Journal of Radioanalytical and Nuclear Chemistry, 2014. **300**(2): p. 547-552.
16. Chilian, C., C. Cimpan, and G. Kennedy, *Contribution of detection efficiency to the uncertainty budget in NAA.* Journal of Radioanalytical and Nuclear Chemistry, 2016. **309**(1): p. 249-255.
17. *REE-2 Certificate of Analysis*. 2016; Available from: https://www.nrcan.gc.ca/node/18270/.
18. Kennedy, G. and J. St-Pierre, *Parameterization of detector efficiency for the standardization of NAA with stable low flux reactors.* Journal of radioanalytical and nuclear chemistry, 1997. **215**(2): p. 235-239.
19. Stosch, H.-G., *Neutron Activation Analysis of the Rare Earth Elements (REE) – With Emphasis on Geological Materials*, in *Physical Sciences Reviews*. 2016.
20. Glascock, M., et al., *Correcting for uranium fission in instrumental neutron activation analysis of high-uranium rocks.* Journal of Radioanalytical and Nuclear Chemistry, 1986. **99**(1): p. 121-131.
21. *X-Ray Mass Attenuation Coefficients*; Available from: *http://www.nist.gov/pml/data/xraycoef/*
22. Guide, I., *13528 (2005) Statistical methods for use in proficiency testing by interlaboratory comparisons.* ISO, Geneva.

CHAPTER 6 GENERAL DISCUSSION AND COMPLEMENTARY NAA RESULTS

This study was part of the REE group research project aiming to develop methods for recovery of the rare earth elements in collaboration with Niobec. These methods include physical beneficiation, extraction and individual separation of rare earth elements.

Along with the objective of the present study for improving the k_0-NAA for detection of rare earth elements, k_0-NAA was considered as one of the main analytical technique for the samples generated in the group project.

Due to the confidentiality of most of these projects, further details concerning their processes cannot be presented. A few selective results are presented in this chapter serving as an example.

6.1 Fresh ore and concentrated ore

The fresh ore and concentrated ore were used as the feed for the processes.

Table 6-1 Elemental analysis of fresh ore for different particle size (µm) measured with k_0-NAA at SLOWPOKE

	Concentration (mg kg^{-1})						
Element	<37	37-53	53-63	63-90	90-106	106-125	125-150
Na*	296	386	352	339	364	736	285
Mg	60038	56535	56322	62588	60639	57439	59141
Al*	3902	4159	4174	6999	4376	5521	3633
Cl**	686	803	831	880	656	724	688
Ca	177110	175992	180584	202347	176457	177559	180463
Sc	46	48	48	45	45	46	46
Mn	12229	11889	11898	11884	11813	11578	11783
Fe**	105493	118468	112346	103649	100803	99587	103518
La	4806	5162	5039	5316	5128	5628	5292
Ce	10205	11256	10552	11051	10250	11873	11305
Pr	1034	1139	1087	1164	1113	1199	1146
Nd*	4999	5126	5043	5218	4879	5016	4776
Sm	388	403	378	418	404	434	394
Eu	95	91	88	90	86	100	96
Gd**	115	217	97	154	128	<140	<200
Tb	13	14	13	14	13	14	13
Dy*	47	46	41	53	43	45	43
Th	597	636	590	671	623	695	627
U	<8	<12	<6	<6	<6	<7.7	<6

Data are presented with uncertainty less than 5%, *less than 10%, **less than 20%

Table 6-2 Elemental analysis of concentrated ore measured with k_0-NAA at SLOWPOKE

	Concentration (mg kg^{-1})				
Element	Sample 1	Sample 2	Sample 3	Sample4	Sample 5
Na*	754	609	927	740	563
Mg	29272	39068	24649	26389	28834
Al*	2592	2076	2390	2621	2385
Cl**	987.6	540	938.4	955.2	888
Ca	100505	123717	87801	83688	102484
Sc*	36	39	33	29	35
Ti	1937	1556	1777	2034	1456
V	52.3	53	51.7	51.9	53.8
Mn	6625	7653	5307	5771	7038
Fe**	88465	97421	<83000	81912	60725
Ag	624	507	562	503	412
In	0.98	0.54	0.65	0.79	0.84
Ba	9891	8684	7714	8670	8873
La	57169	47673	68890	66805	55209
Ce	111138	89424	125113	121047	109910
Nd	34052	26589	37627	35035	33761
Sm	4125	3484	4966	4744	3989
Eu	977	649	977	980	887
Gd**	1707	1803	2308	2118	2413
Dy	387	319	491	458	341
Yb**	121	109	117	136	93
Th	5597	4397	6162	5888	5526
U**	24	17	24	21	18

Data are presented with uncertainty less than 5%, *less than 10%, **less than 20%

6.2 Beneficiation of fresh ore: Froth flotation

One of the processes in physical beneficiation was froth flotation. A description of this process is presented along with a series of results obtained by k_0-NAA.

500 grams of fresh ore (P80 = 106 µm) was ground wet in a ball mill in order to obtain a P80 of 53 µm. The slurry was transferred to a 1.2 L flotation cell and was added to more water to obtain a 30 % solid slurry. The pH of the slurry is then modified to the desired pH before conditioning with the collector and frother. The air was introduced and as soon as the froth appeared, it was scraped to a collecting tray. Flotation was conducted for a total of 10 min, collecting different concentrations at different times. The tailings were filtered in a vacuum filter, and were dried along with the concentrates in the laboratory oven.

Table 6-3 Elemental analysis of selected samples from flotation process with k_0-NAA at SLOWPOKE

Sample code	Concentration (mg kg^{-1})									
	La	Ce	Pr	Nd	Sm	Fe	Mn	Al*	Mg	Ca
MG10	7238	12992	1294	4290	280	95407	12772	2818	71859	131281
MG11	5698	10203	999	3333	219	102949	13317	2304	70683	135781
MG12	16378	30442	2879	9640	657	98808	10904	4555	60906	117883
MG13	24793	46132	4373	15098	965	106626	9893	8940	67442	112529
MG14	22241	41215	4260	13755	825	109618	10209	5330	60193	101590
MG15	25930	48904	2720	16407	1052	105339	8982	5619	56087	86782
MG16	26061	50069	4200	16434	1084	127128	9284	6089	56180	93096
MG17	21278	39643	1000	12728	858	105716	10171	5612	60725	102771
MG18	18236	33804	3700	11277	736	106380	10570	5286	60703	108081

Table 6-4 Metal content considering the k_0-NAA result and the mass of the samples

Sample code	Mass, (g)	Metal content, %									
		La	Ce	Pr	Nd	Sm	Fe	Mn	Al*	Mg	Ca
MG10	500.81	3.62	6.51	0.65	2.15	0.14	47.78	6.40	1.41	35.99	65.75
MG11	443.33	2.53	4.52	0.44	1.48	0.10	45.64	5.90	1.02	31.34	60.20
MG12	16.38	0.27	0.50	0.05	0.16	0.01	1.62	0.18	0.07	1.00	1.93
MG13	9.72	0.24	0.45	0.04	0.15	0.01	1.04	0.10	0.09	0.66	1.09
MG14	9.92	0.22	0.41	0.04	0.14	0.01	1.09	0.10	0.05	0.60	1.01
MG15	5.2	0.13	0.25	0.01	0.09	0.01	0.55	0.05	0.03	0.29	0.45
MG16	2.84	0.07	0.14	0.01	0.05	0.00	0.36	0.03	0.02	0.16	0.26
MG17	5.32	0.11	0.21	0.01	0.07	0.00	0.56	0.05	0.03	0.32	0.55
MG18	5.08	0.09	0.17	0.02	0.06	0.00	0.54	0.05	0.03	0.31	0.55
Calculated MG10		3.67	6.66	0.63	2.18	0.14	51.39	6.46	1.34	34.67	66.04
Difference, %		1.27	2.33	3.52	1.28	1.41	7.56	1.01	5.12	3.67	0.45

MG10 is the feed sample, MG11 – MG18 are the samples in the product. Hence, the sum of MG11 – MG18 should give the value of MG10

$$\%\text{difference} = \frac{|\text{calculated} - \text{measured}|}{\text{measured}} \times 100 \tag{6-1}$$

In addition to REE-2, a certified reference material from the Institute for Reference Materials and Measurements (IRMM) was tested with k_0-NAA. The results are presented in

Table **6-5**.

Table 6-5 Comparison of REE concentrations measured with k_0-NAA (X_{lab}) with respect to certified values (X_{cer}) for Estuarine sediment, BCR-667

Element	X_{cer}	$\pm u_{cer}$(mg kg^{-1})	X_{lab}	$\pm u_{lab}$(mg kg^{-1})	X_{lab}/X_{cer}
La	27.8	±1	26.9	±1.2	0.97
Ce	56.7	±2.5	54.2	±2.7	0.96
Pr	6.1	±0.5	5.9	±0.3	0.97
Nd	25	±1.4	<32	-	-
Sm	4.66	±0.2	4.74	±0.2	1.02
Eu	1	±0.05	1.01	±0.1	1.01
Gd	4.41	±0.12	<10	-	-
Tb	0.682	±0.017	0.72	±0.04	1.06
Dy	4.01	±0.14	3.96	±0.2	0.99
Ho	0.80	±0.06	0.72	±0.07	0.90
Er	2.35	±0.15	<10	-	-
Tm	0.325	±0.025	<5	-	-
Yb	2.20	±0.09	2.06	±0.10	0.94
Lu	0.325	±0.02	0.300	±0.02	0.92

CHAPTER 7 CONCLUSION AND RECOMMENDATIONS

In this research work, we investigated k_0-NAA's capability for determining of rare earth elements in highly concentrated samples. Factors affecting REE measurement with k_0-NAA were assessed theoretically and experimentally.

Values for k_0 and Q_0 along with the detection efficiency model were experimentally validated with the use of mono rare earth standard solutions and corrected when necessary. As for ^{169}Yb (177 and 198 keV) and ^{177}Lu (208 keV), further study is needed over k_0 and Q_0 data. Inconsistencies in correcting the true coincidence summing effects indicated that COI factors are not accurate and further improvements are needed.

The spectral and nuclear interferences were investigated experimentally or calculated theoretically. Correction factors for spectral interferences induced by rare earth elements, thorium, uranium and from uranium fission products were determined and added to the EPAA libraries.

The performance of gamma-ray self-attenuation coupled with the neutron self-shielding iterative calculation was assessed by using rare earth oxide standards and it showed sufficient accurate results for cases with 67% combined effects.

The improved k_0-NAA was applied to determine the REE content in certified reference material and the results showed good agreement with reported certified values within the range of the estimated uncertainty. This findings validated the new method indicating that 10 REEs can be accurately measured by k_0-NAA at the Polytechnique Montreal NAA Laboratory with a turnaround time of 8 days.

Further improvements can be done in order to be able to determine 12 REE in concentrated samples with short analytical turnaround times.

During the present study more than 300 REE samples were analysed for the NSERC-CRD project.

BIBLIOGRAPHY

1. Connelly, N.G., *Nomenclature of inorganic chemistry: IUPAC recommendations 2005*. 2005: Royal Society of Chemistry.
2. Gupta, C. and N. Krishnamurthy, *Extractive metallurgy of rare earths.* International Materials Reviews, 1992. **37**(1): p. 197-248.
3. Krishnamurthy, N. and C.K. Gupta, *Extractive metallurgy of rare earths*. 2004: CRC press.
4. Spedding, F., *Contributions to the rare earths to science and technology*. 1975, Ames Lab., Iowa (USA).
5. Jordens, A., Y.P. Cheng, and K.E. Waters, *A review of the beneficiation of rare earth element bearing minerals.* Minerals Engineering, 2013. **41**: p. 97-114.
6. Chi, R., et al. *Beneficiation of rare earth ore in china*. in *Light Metals 2001 as held at the 130 th TMS Annual Meeting*. 2001.
7. Wübbeke, J., *Rare earth elements in China: Policies and narratives of reinventing an industry.* Resources Policy, 2013. **38**(3): p. 384-394.
8. Humphries, M., *Rare earth elements: the global supply chain*. 2010: DIANE Publishing.
9. Bulska, E., et al., *Inductively coupled plasma mass spectrometry in comparison with neutron activation and ion chromatography with UV/VIS detection for the determination of lanthanides in plant materials.* Talanta, 2012. **97**: p. 303-311.
10. Dybczyński, R.S., et al., *Comparison of performance of INAA, RNAA and ion chromatography for the determination of individual lanthanides.* Applied Radiation and Isotopes, 2010. **68**(1): p. 23-27.
11. Santoro, A., et al., *Assessing rare earth elements in quartz rich geological samples.* Applied Radiation and Isotopes, 2016. **107**: p. 323-329.
12. D'Angelo, J.A., et al., *Determination of eight lanthanides in apatites by ICP-AES, XRF, and NAA.* Journal of trace and microprobe techniques, 2001. **19**(1): p. 79-90.
13. Zawisza, B., et al., *Determination of rare earth elements by spectroscopic techniques: a review.* Journal of Analytical Atomic Spectrometry, 2011. **26**(12): p. 2373-2390.
14. Whitty-Léveillé, L., et al., *A comparative study of sample dissolution techniques and plasma-based instruments for the precise and accurate quantification of REEs in mineral matrices.* Analytica Chimica Acta, 2017. **961**: p. 33-41.
15. Tiwari, S., et al., *Analysis of uranium bearing samples for rare earth and other elements by k0-based internal monostandard INAA method.* Journal of Nuclear and Radiochemical Sciences, 2007. **8**(1): p. 25-30.
16. Ravisankar, R., et al., *Determination and distribution of rare earth elements in beach rock samples using instrumental neutron activation analysis (INAA).* Nuclear Instruments and Methods in Physics Research Section B: Beam Interactions with Materials and Atoms, 2006. **251**(2): p. 496-500.
17. Wasim, M., S. Iqbal, and M. Ali, *Radiological and elemental analysis of soils from Hunza in Central Karakoram using gamma-ray spectrometry and k0-instrumental neutron activation analysis.* Journal of Radioanalytical and Nuclear Chemistry, 2016. **307**(2): p. 891-898.

18. Xiao, C., et al., *k0-NAA for determination of REE in reference materials of ore sources.* Journal of Radioanalytical and Nuclear Chemistry, 2017. **311**(2): p. 1287-1289.
19. Hevesy, G. and H. Levi, *The Action of Neutrons on the Rare Earth Elements. Det.* Kgl. Danske videnska-pernes selskab. Matematisk-fysiske meddelelser, 1936. **14**(5).
20. Hevesy, G.d. and H. Levi, *Action of slow neutrons on rare earth elements.* Nature, 1936. **137**(3457): p. 185.
21. Shulyakova, O., P. Avtonomov, and V. Kornienko, *New developments of neutron activation analysis applications.* Procedia-Social and Behavioral Sciences, 2015. **195**: p. 2717-2725.
22. ; Available from: http://nmi3.eu/neutron-research/techniques-for-/chemical-analysis.html.
23. Stosch, H.-G., *Neutron Activation Analysis of the Rare Earth Elements (REE) – With Emphasis on Geological Materials,* in *Physical Sciences Reviews*. 2016.
24. van Sluijs, R., *Q 0's and resonance energies used in k 0-NAA compared with estimations based on ENDF/B-VII. 1 cross section data.* Journal of Radioanalytical and Nuclear Chemistry, 2016. **309**(1): p. 219-228.
25. Pommé, S., et al., *Neutron activation analysis with k 0-standardisation: general formalism and procedure*. 1997, Centre de l'Etude de l'Energie Nucleaire.
26. Bereznai, T., *Methods, problems and trends of standardization in multielement reactor neutron activation analysis.* Fresenius' Journal of Analytical Chemistry, 1980. **302**(5): p. 353-363.
27. Kafala, S. and T. MacMahon, *Comparison of neutron activation analysis methods.* Journal of radioanalytical and nuclear chemistry, 2007. **271**(2): p. 507-516.
28. De Corte, F., *The k 0 Standardization Method-a Move to the Optimization of NAA.* Rijksuniversiteit Gent, 1987.
29. Arboccò, F.F., et al., *Experimental determination of k0, Q0 factors, effective resonance energies and neutron cross-sections for 37 isotopes of interest in NAA.* Journal of Radioanalytical and Nuclear Chemistry, 2014. **302**(1): p. 655-672.
30. *k0-International Scientific Committee (2012) Classic k0 Database. International*. 2012; Available from: http://www.icaa-mtaa.org/k0data/Shared%20Documents/DataBases/Excel_2012_03_14/k0_database_2012_03_14.xls.
31. Jaćimović, R., et al., *The 2012 recommended k0 database.* Journal of Radioanalytical and Nuclear Chemistry, 2014. **300**(2): p. 589-592.
32. Kennedy, G. and J. St-Pierre, *Is the k0 method accurate for elements with high Q0 values?* Journal of radioanalytical and nuclear chemistry, 2003. **257**(3): p. 475-480.
33. St-Pierre, J. and G. Kennedy, *Re-measurement of Q 0 and k 0 values for 14 nuclides.* Nuclear Instruments and Methods in Physics Research Section A: Accelerators, Spectrometers, Detectors and Associated Equipment, 2006. **564**(2): p. 669-674.
34. Westcott, C., *Effective cross section values for well-moderated thermal reactor spectra.(corrected)*. 1960, Atomic Energy of Canada Ltd., Chalk River, Ontario (Canada).
35. Hamidatou, L., et al., *Concepts, Instrumentation and Techniques of Neutron Activation Analysis,* in *Imaging and Radioanalytical Techniques in Interdisciplinary Research-Fundamentals and Cutting Edge Applications*. 2013, InTech.
36. *Canadian Nuclear Safety Commission*. Available from: http://nuclearsafety.gc.ca/eng/.
37. Reguigui, N., *Gamma Ray Spectrometry.* 2006.

38. Rittersdorf, I., *Gamma ray spectroscopy.* Nuclear Engineering & Radiological Sciences, 2007: p. 18-20.
39. Gordon, G.E., et al., *Instrumental activation analysis of standard rocks with high-resolution γ-ray detectors.* Geochimica et Cosmochimica Acta, 1968. **32**(4): p. 369-396.
40. Duffield, J. and G. Gilmore, *An optimum method for the determination of rare earth elements by neutron activation analysis.* Journal of Radioanalytical and Nuclear Chemistry, 1979. **48**(1-2): p. 135-145.
41. Dampare, S., et al., *Determination of rare earth elements by neutron activation analysis in altered ultramafic rocks from the Akwatia District of the Birim diamondiferous field, Ghana.* Journal of Radioanalytical and Nuclear Chemistry, 2005. **265**(1): p. 101-106.
42. El-Taher, A., *Rare earth elements content in geological samples from eastern desert, Egypt, determined by instrumental neutron activation analysis.* Applied Radiation and Isotopes, 2010. **68**(9): p. 1859-1863.
43. Akinlua, A., et al., *Rare earth element geochemistry of petroleum source rocks from northwestern Niger Delta.* Marine and Petroleum Geology, 2016. **77**: p. 409-417.
44. Ashraf, A., et al., *Rare earth elements in core marine sediments of coastal East Malaysia by instrumental neutron activation analysis.* Applied Radiation and Isotopes, 2016. **107**: p. 17-23.
45. Danko, B., R. Dybczyński, and Z. Samczyński, *Accurate determination of individual lanthanides in biological materials by NAA with pre-and post-irradiation separation.* Journal of radioanalytical and nuclear chemistry, 2008. **278**(1): p. 81-88.
46. Silachyov, I., *Rare earths analysis of rock samples by instrumental neutron activation analysis, internal standard method.* Journal of Radioanalytical and Nuclear Chemistry, 2016. **310**(2): p. 573-582.
47. Chilian, C. and G. Kennedy, *The NAA method at Polytechnique Montreal: an efficient alternative way to use the k0 NAA models.* Journal of Radioanalytical and Nuclear Chemistry, 2014. **300**(2): p. 533-538.
48. Simonits, A., et al., *ko-measurements and related nuclear data compilation for (n, γ) reactor neutron activation analysis.* Journal of Radioanalytical and Nuclear Chemistry, 1980. **60**(2): p. 461-516.
49. Simonits, A., et al., *Status and recent developments in the k0-standardization method.* Journal of Radioanalytical and Nuclear Chemistry, 1982. **72**(1-2): p. 209-230.
50. Moens, L., et al., *k0-measurements and related nuclear data compilation for (n, γ) reactor neutron activation analysis: Part II.* Journal of Radioanalytical and Nuclear Chemistry, 1984. **82**(2): p. 385-452.
51. De Corte, F. and A. Simonits, *k0-Measurements and related nuclear data compilation for (n, γ) reactor neutron activation analysis: IIIb: Tabulation*. Journal of radioanalytical and nuclear chemistry, 1989. **133**(1): p. 43-130.
52. De Soete, R.G.a.J.H., *Neutron Activation Analysis: John Wiley, New York, 1972*. 1973, Elsevier.
53. Arboccò, F.F., et al., *Experimental validation of some thermal neutron self-shielding calculation methods for cylindrical samples in INAA.* Journal of Radioanalytical and Nuclear Chemistry, 2012. **291**(2): p. 529-534.

54. Chilian, C., J. St-Pierre, and G. Kennedy, *Complete thermal and epithermal neutron self-shielding corrections for NAA using a spreadsheet.* Journal of radioanalytical and nuclear chemistry, 2008. **278**(3): p. 745-749.
55. Case, K.M., G. Placzek, and F. Hoffmann, *Introduction to the theory of neutron diffusion, v. 1.* 1953.
56. Dwork, J., et al., *Self-shielding factors for infinitely long, hollow cylinders*. 1955, Knolls Atomic Power Lab.
57. Nisle, R.G., *A Neutron Absorption Alignment Chart*. 1957, Phillips Petroleum Co. Atomic Energy Div., Idaho Falls, Idaho.
58. Stewart, J. and P. Zweifel, *ABSORPTION OF NEUTRONS.* Progress in Nuclear Energy: Physics and mathematics, 1959. **3**: p. 331.
59. Gilat, J. and Y. Gurfinkel, *Self-shielding in activation analysis.* Nucleonics (US) Ceased publication, 1963. **21**(8).
60. Fleming, R.F., *Neutron self-shielding factors for simple geometrics.* The International Journal of Applied Radiation and Isotopes, 1982. **33**(11): p. 1263-1268.
61. Dodoo-Amoo, D. and S. Landsberger, *Gamma-ray self attenuation calculations in neutron activation ananlysis: A problem overlooked.* Journal of Radioanalytical and Nuclear Chemistry, 2001. **248**(2): p. 327-332.
62. Robu, E. and C. Giovani, *Gamma-ray self-attenuation corrections in environmental samples.* Romanian Reports in Physics, 2009. **61**(2): p. 295-300.
63. Al Attar, L., et al., *Evaluation of Self-attenuation Coefficients of Oil-Produced Scales For Gamma-Ray Spectroscopic Analysis.* Instrumentation Science & Technology, 2014. **42**(5): p. 562-575.
64. Nelson, G. and D. Reilly, *Gamma-ray interactions with matter.* Passive nondestructive analysis of nuclear materials, 1991: p. 27-42.
65. Sima, O., D. Arnold, and C. Dovlete, *GESPECOR: a versatile tool in gamma-ray spectrometry.* Journal of Radioanalytical and Nuclear Chemistry, 2001. **248**(2): p. 359-364.
66. *REE-2 Certificate of Analysis*. 2016; Available from https://www.nrcan.gc.ca/node/18270/.
67. *X-Ray Mass Attenuation Coefficients.* http://www.nist.gov/pml/data/xraycoef/.